Laser-Doppler versus ultrasound measurements of pulsatile flow in a distensible tube

Slegers, H.J.

Award date:
1995

Laser-Doppler versus ultrasound measurements of pulsatile flow in a distensible tube

H.J. Slegers, march 1995
WFW reportnr. 95–040

Afstudeerrapport,

Begeleiders:	Dr.Ir. F.N. van de Vosse Ir. M.C.M. Rutten
Hoogleraren:	Prof.Dr.Ir. M.E.H. van Dongen Prof.Dr.Ir. J.D. Janssen

Contents

Abstract

In the first period of this study an experimental setup has been developed in which local velocity in and wall displacement of a distensible tube can be measured under pulsatile flow conditions using both laser-Doppler and ultrasound techniques. In order to create physiological pressure-flow relations in the tube, the experimental setup is terminated with a hydraulic load that mimics the behavior of the arterial system distal to the arterial segment that is modelled. The hydraulic load has been constructed, based on a four-element Windkessel model. Its parameters can be adjusted in a reproducable way.

In the second period of this study the experimental setup was scaled 1:1 for a thoracic aorta. Velocity profiles, pressure, flow inside and distension of the tube have been measured at several positions along the tube axis using both laser-Doppler and Ultrasound techniques. These measurements have been conducted in close cooperation with the University of Limburg, department of biophysics, where the ultrasound equipment has been developed. A comparison has been made between the velocity profiles obtained from laser-Doppler anemometry and those obtained from the ultrasound measurements. The spatial resolution of both techniques was found to be comparable and in general, a good agreement between the results obtained by both techniques was found. Wall distension was measured with ultrasound and a laser-vibrometer. A difference was found in the distension in horizontal and vertical direction. Moreover, a significant difference was found between ultrasound and laser-vibrometer measurements.

Furthermore impedance was determined in terms of distension and center-line velocity. The university of Limburg intends to use this method in clinical practice to determine impedance in the human arterial system. The measurements show that for the configuration used in this study, impedance determined in this way is in rather good agreement with impedance determined from pressure and flow.

Finally the experimental setup was modelled with a linear wave propagation model for distensible tubes, which incorporates reflection. Calculated pressure, flow inside and distension of the tube are in good agreement with measured pressure, flow and distension.

Chapter 1

Introduction

Atherosclerosis is a disease of the larger arteries and is one of the most important causes of death in the western world. The disease is characterised by a stiffening and thickening of the blood vessel wall. It is now generally assumed that the development and the location of atherosclerosis is related to the flow induced wall shear that locally exists [Fri93].

The objective of this study is to build an experimental setup in which local wall shear can be determined from measurements of local velocity and wall displacement in a distensible tube under pulsatile flow conditions using laser-Doppler and ultrasound techniques. As the velocity profiles and wall shear stress strongly depend on the flow wave through the setup, the entry flow must be of physiological relevance. Moreover the terminal impedance of the experimental setup must be modelled correctly in order to obtain a physiogically relevant pressure-flow relationship and hereby a physiologically relevant wall motion. Because atherosclerosis mainly appears in the larger arteries such as the aorta, renal, carotid and coronary arteries, the experimental setup should reproduce pressure-flow relations in these arteries correctly.

In order to design the experimental setup first a linear model was designed for pulsatile flow through a distensible tube. The terminal load is modelled using a four-element Windkessel model, see chapter 2. Based on this four-element Windkessel model a hydraulic load is constructed and tested, see appendix B. Reflections occuring from the the transition from tube to hydraulic load are incorporated in the model. In chapter 3 measurements of velocity profiles in and distension of the tube under physiological flow conditions using laser-Doppler and ultrasound techniques are described. The results of these measurements are reported in chapter 4 and compared with the model derived in chapter 2. The final chapter is devoted to a discussion of the results.

Chapter 2

Arterial modelling

After a short physiological introduction, in this chapter a model is derived that describes physiological pressure-flow relationships in an arterial segment. First a model describing blood flow and wave propagation in arterial segments is discussed (section 2.2). Next the concept of input impedance is introduced in section 2.3 in order to derive a model for the terminal load of arterial segments (section 2.4). Lastly reflections will be incorporated in the model.

2.1 The circulatory system

The circulation of blood in humans can be separated into two major systems: the systemic circulation and the pulmonary circulation. The *systemic circulation* supplies blood to all organs and tissues of the body and can be divided into two parts: the arterial system and the venous system. The *arterial system* consists of blood vessels of various length and diameter that successively branch into smaller vessels (table 2.1). The blood, rich in oxygen, leaves the heart and flows into the arterial system through the aorta, the largest artery in the body. The aorta branches into smaller blood vessels (arteries and arterioles) until the capillary beds are reached. An important characteristic of the arterial system with respect to arterial modelling is the stiffening of the blood vessels as the distance from the heart increases. The capillary beds are formed by a mesh of very small vessels (capillaries) where the exchange of nutritiants and waste in organs takes place. After this the blood, rich in carbon dioxide, enters the *venous system*. The capillaries join together into the venules and veins and end where the vena cava enters the heart. The veins

vessel	average diameter	wall thickness
aorta	2.5 cm	2 mm
arteries	0.4 cm	1 mm
arterioles	30 μm	20 μm
capillaries	6 μm	1 μm
venules	20 μm	2 μm
veins	0.5 cm	0.5 mm
vena cava	3 cm	1.5 mm

Table 2.1: *Geometric properties of different blood vessels in man [Din81].*

operate in a much lower pressure area than arteries at the same level, the vessel walls of veins are thinner and many veins contain valves which prevent backflow of blood.

Finally the blood is pumped into the *pulmonary circulation*, which supplies blood to the lungs, where filtration of carbon dioxide and supply of oxygen takes place. Blood then flows back to the heart and enters the systemic circulation again. The supply of blood to the heart itself is carried out by two main coronary arteries that branch off the aorta.

2.2 Modelling blood flow in arterial segments

In the first subsection an equation of motion for blood flow in arterial segments will be derived. Next a quasi one-dimensional wave propagation model will be derived.

2.2.1 Equations of motion

To describe blood flow in an arterial segment we simplify the Navier-Stokes equations by assuming that blood behaves like a Newtonian fluid and that the arterial segment can be considered as a homogeneous isotropic elastic tube with radius R. Furthermore by assuming an axi-symmetric velocity profile we can write the momentum equation in cylindrical coordinates as:

$$-\frac{1}{\rho}\frac{\partial p}{\partial x} = \frac{\partial u_x}{\partial t} + u_r\frac{\partial u_x}{\partial r} + u_x\frac{\partial u_x}{\partial x} - \nu(\frac{\partial^2 u_x}{\partial r^2} + \frac{1}{r}\frac{\partial u_x}{\partial r} + \frac{\partial^2 u_x}{\partial x^2}) \tag{2.1}$$

Under these assumptions the continuity equation can be written as:

$$\frac{1}{r}\frac{\partial}{\partial r}(ru_r) + \frac{\partial u_x}{\partial x} = 0 \tag{2.2}$$

Due to distensibility of the tube, pressure and flow waves will propagate with a finite wave speed c and a typical wavelength λ. First a properly scaled dimensionless form of the Navier-Stokes equation is derived. The radial coordinate is made dimensionless using the mean radius of the tube, i.e. $r' = r/R_o$. The axial coordinates are scaled with the wavelength: $x' = x/\lambda$. The axial velocity is made dimensionless with its characteristic value over a cross-section, i.e. $u'_x = u_x/U$. From the continuity equation it follows that the radial velocity is scaled as: $u'_r = (u_r\lambda)/(UR_o)$. The characteristic time $t' = \omega t$ can be written as $t' = (c/\lambda)t$. Finally the pressure is made dimensionless as: $p' = p/(\rho Uc)$. Assuming that the longitudinal velocity u_x is small in comparison with the wave speed c in the blood vessel and assuming long waves (blood vessel radius R much smaller than wavelength λ), the Navier-Stokes equation is reduced to (dropping all primes):

$$\frac{\partial u_x}{\partial t} = -\frac{1}{\rho}\frac{\partial p}{\partial x} + \nu\frac{1}{r}\frac{\partial}{\partial r}(r\frac{\partial u_x}{\partial r}) \tag{2.3}$$

The continuity equation does not change in form. If we search for harmonic solutions with angular frequency ω and wave number k:

$$p = \hat{p}e^{i(\omega t - kx)} \tag{2.4}$$

$$u_x = \hat{u}_x(r)e^{i(\omega t - kx)} \tag{2.5}$$

substitution in equation (2.3) yields the same differential equation for $\hat{u}_x$ as in the case of a rigid tube. Equations (2.4) and (2.5) assume that the system is linear in behavior and that no reflected waves are present. Assuming that the wall motion is axially restrained gives exactly the same solution for $\hat{u}_x$ as in the case of a rigid tube, equation (A.12). The wavenumber k has still to be determined.

2.2.2 Wave propagation in distensible tubes

Now a quasi one-dimensional wave propagation model for pressure and flow waves will be derived. The momentum (2.3) and continuity equation (2.2) are integrated over the radius using the Leibnitz formula. If Ω is a moving region with boundary Γ and $\vec{v}_\Gamma$ the velocity of the moving boundary, the Leibnitz formula is:

$$\frac{d}{dt}\int\limits_{\Omega(t)} s d\Omega = \int\limits_{\Omega(t)} \frac{\partial s}{\partial t} d\Omega + \int\limits_{\Gamma(t)} s(\vec{v}_\Gamma \cdot \vec{n}) d\Gamma = 0 \tag{2.6}$$

Application of the Leibnitz formula to the second term in the continuity equation integrated over the radius:

$$2\pi \left[\int\limits_0^{R(x,t)} \frac{1}{r}\frac{\partial}{\partial r}(r u_r) r dr + \int\limits_0^{R(x,t)} \frac{\partial u_x}{\partial x} r dr \right] = 0 \tag{2.7}$$

yields:

$$2\pi \int\limits_0^{R(x,t)} \frac{\partial r u_r}{\partial r} dr + 2\pi \frac{\partial}{\partial x} \int\limits_0^{R(x,t)} u_x r dr - 2\pi u_x r|_0^R = 0 \tag{2.8}$$

If we assume that the motion of the wall is longitudinally restrained, i.e. $u_x(R,t) = 0$ we obtain:

$$2\pi r u_r|_0^R + \frac{\partial Q}{\partial x} = 0 \tag{2.9}$$

Rewriting the first term in terms of the cross-sectional area $A(x,t) = \pi R^2(x,t)$ gives:

$$\frac{\partial A}{\partial t} + \frac{\partial Q}{\partial x} = 0 \tag{2.10}$$

The momentum equation in axial direction can be integrated in a similar way:

$$2\pi \int\limits_0^{R(x,t)} \frac{\partial u_x}{\partial t} r dr = -2\pi \int\limits_0^{R(x,t)} \frac{1}{\rho}\frac{\partial p}{\partial x} r dr + 2\pi\nu \int\limits_0^{R(x,t)} \frac{\partial}{\partial r}(r\frac{\partial u_x}{\partial r}) dr \tag{2.11}$$

Application of the Leibnitz formula to the first term yields:

$$2\pi \frac{\partial}{\partial t} \int\limits_0^{R(x,t)} u_x r dr - 2\pi u_x u_r r|_0^R = -\frac{A}{\rho}\frac{\partial p}{\partial x} + 2\pi\nu r \frac{\partial u_x}{\partial r}|_0^R \tag{2.12}$$

The second term vanishes because of the longitudinal restraint of the wall motion. The last term in the right hand side can be written in terms of the wall shear stress $\tau = -\eta \frac{\partial u_x}{\partial r}|_{r=R}$:

$$\rho\frac{\partial Q}{\partial t} + A\frac{\partial p}{\partial x} = -\frac{2A\tau}{R} \tag{2.13}$$

Together with the expression for the wall shear stress (equation (A.20)) and linearisation of the $A\frac{\partial p}{\partial x}$ term this finally gives:

$$\rho\frac{\partial Q}{\partial t} + A_o\frac{\partial p}{\partial x} = -f_0 Q \tag{2.14}$$

with f_0 the friction function:

$$f_0(\omega) = i\omega\rho\frac{F_{10}(\omega)}{1 - F_{10}(\omega)} \tag{2.15}$$

and F_{10} is a complex function of the Bessel function of the zero-th and first order (equation (A.17)). Equations (2.14) and (2.10) can be solved in the frequency domain due to the assumed linearity by substituting harmonic solutions:

$$p(\omega, x, t) = \hat{p}(\omega, 0)e^{i(\omega t - kx)} \tag{2.16}$$
$$Q(\omega, x, t) = \hat{Q}(\omega, 0)e^{i(\omega t - kx)} \tag{2.17}$$
$$A(\omega, x, t) = \hat{A}(\omega, 0)e^{i(\omega t - kx)} \tag{2.18}$$

where $\hat{p}(\omega, 0)$ are the complex amplitudes at location $x = 0$ with angular frequency ω. The wavenumber is denoted by $k(\omega)$ and is defined by:

$$k(\omega) = \frac{\omega}{c} - i\frac{\gamma(\omega)}{\lambda} \tag{2.19}$$

where c denotes the phase velocity of the waves. The exponential decrease of the wave is described by the attenuation constant γ. Wall behavior is described by a relationship between cross-sectional area $\hat{A}$ and pressure $\hat{p}$:

$$\hat{A} = C'(\omega)\hat{p} \tag{2.20}$$

with $C'(\omega)$ the dynamic compliance. Substituting equations (2.16)– (2.18), (2.20) and (2.15) in equations (2.10) and (2.14) results in an expression for the wave number:

$$k(\omega) = \pm\frac{\omega}{c_0}\sqrt{\frac{1}{1 - F_{10}(\omega)}} \tag{2.21}$$

with c_0 the Moens-Korteweg wave speed:

$$c_0(\omega) = \sqrt{\frac{\pi {R_o}^2}{\rho C'(\omega)}} \tag{2.22}$$

2.3 Impedance

To describe the behavior of the arterial system and to provide data for the *in-vitro* setup, it is necessary to obtain relationships between pressure and flow. Commonly used for this purpose is the quantity *input impedance*, which is a special case of a system description in the frequency domain, and can therefore only be used in linear systems. Impedance is determined from simultaneously measured pressure and flow (which are periodic) at the same location in the arterial system. These signals are decomposed into several harmonics (N) by means of Fourier analysis. The pressure, $p(t)$, and flow, $Q(t)$, can now be represented by a (complex) Fourier series:

$$p(t) = \sum_{i=0}^{N} \hat{p}_i e^{j\omega_i t} \tag{2.23}$$

$$Q(t) = \sum_{i=0}^{N} \hat{Q}_i e^{j\omega_i t} \tag{2.24}$$

where $i(= 0, 1, 2, ..)$ denotes the harmonic under consideration, $\omega_i = 2\pi i f_{heart}$, and $\hat{p}_i$ and $\hat{Q}_i$ are the complex amplitudes of pressure and flow. A complex amplitude consists of a modulus and phase angle. The impedance for the i-th harmonic is obtained by division of the corresponding complex pressure and flow amplitudes:

$$Z_i = \frac{\hat{p}_i}{\hat{Q}_i} \tag{2.25}$$

For $i = 0$, equation (2.25) represents the ratio of the mean pressure and mean flow, commonly called *vascular resistance* [Att66]. Besides input impedance there are three other definitions of impedance, which depend on the local characteristics of the arterial segment under consideration:

- *longitudinal impedance:* defined as the ratio of the pressure gradient to flow at one location of a segment of artery:

$$Z'_L = -\frac{\partial \hat{p}}{\partial x}/\hat{Q} \tag{2.26}$$

- *transverse impedance:* defined as the ratio of the transmural pressure difference and volume change of a segment of artery:

$$Z'_T = -\hat{p}/\frac{\partial \hat{Q}}{\partial x} \tag{2.27}$$

- *characteristic impedance:* defined as the input impedance of an "infinitely" long artery with uniform properties, and is independent of the location in this artery.

2.3.1 Longitudinal and transverse impedance

The simplest model of an arterial segment is a cylindrical distensible tube. Pressure-flow relations in a cylindrical distensible tube can be derived by calculating longitudinal impedance for a rigid tube, neglecting all aspects of distensibility. The transverse impedance is then derived for a compliant segment. For an incompressible oscillatory Newtonian fluid flowing in a rigid tube with circular cross-section the longitudinal impedance is (see appendix A):

$$Z'_L = \frac{i\alpha^2}{8}\frac{R'}{1 - F_{10}(\alpha)} \tag{2.28}$$

where R' is the Poiseuille resistance per unit length,

$$R' = \frac{8\eta}{\pi R^4} \tag{2.29}$$

and α is a dimensionless parameter, the Womersley-parameter, which is a measure for the ratio of viscous forces and unsteady inertial forces:

$$\alpha = R\sqrt{\frac{\omega}{\nu}} \tag{2.30}$$

For small arteries or steady flow ($\alpha \cong 0$) the longitudinal impedance reduces to the Poiseuille resistance, i.e. viscous effects are dominant. For high frequencies and large arteries ($\alpha > 10$) the inertial forces dominate the viscous forces and the longitudinal impedance reduces to [Wes77]:

$$Z'_L = \frac{j\omega\rho}{\pi R^2} = j\omega L' \tag{2.31}$$

where L' denotes the effective mass of the blood per cross section.

The transverse impedance of an artery is directly related to the compliance per unit length, which is defined as $C' = dA/dp$. The relation is [Wes77]:

$$Z'_T = \frac{1}{j\omega C'} \tag{2.32}$$

The compliance (per unit length) depends on the characteristics of the artery: for a thin walled elastic tube (wall thickness h, vessel radius R and Young's modulus E of the vessel wall), the compliance is:

$$C' = \sqrt{\frac{2\pi R^3(1-\mu^2)}{Eh}} \tag{2.33}$$

with μ the Poisson's ratio. For large arteries the frequency dependence of the Young's modulus is small, so we can write $E(\omega) = E$. Other models for the compliance can be implemented, for example with a complex Young's modulus (visco-elastic wall behavior).

2.3.2 Characteristic impedance and reflections

The input impedance of an infinitely long artery with constant properties (i.e. a reflectionless system) is defined as the characteristic impedance, Z_C. Changes in the characteristic impedance along an artery leads to reflections in the arterial system. From the theory of wave reflection in tubes, section 2.5, it follows that the input impedance at some location x in the tube can be written as:

$$Z_i(x) = Z_C \cdot \frac{1+\Gamma(x)}{1-\Gamma(x)} \tag{2.34}$$

with $\Gamma(x)$ the reflection coefficient at location x. The reflection coefficient Γ is defined as the ratio of the reflected and forward pressure wave at some location (x) in the arterial system. Equation (2.34) is equivalent to equation (2.46).

2.3.3 Interpretation of input impedance

The modulus of input impedance for the larger blood vessels in all animals show the same behavior: it is relatively large for the zero-th harmonic and then decreases to much lower values for the higher harmonics (approaching the characteristic impedance of the blood vessel). This can be explained from equation (2.34). All waves generated by the heart are partially reflected at the many bifurcations. For low frequencies the returning waves are added in phase because they travelled over only a short distance with respect to their wavelength and total reflection in the system is large (Γ close to unity). From equation (2.34) then follows that the input impedance will be large. For high frequencies the waves return with random phase because they travel distances comparable to or longer than their wavelength. Thus the reflection coefficient is small and the input impedance approaches the characteristic impedance.

The phase angle of the input impedance for larger blood vessels is strongly negative for low frequencies (approaching -90°) and for higher frequencies it approaches zero values, i.e. compliant and inertial effects in the arterial system play a role (see also section 2.4 where a model is presented for the terminal load of arteries).

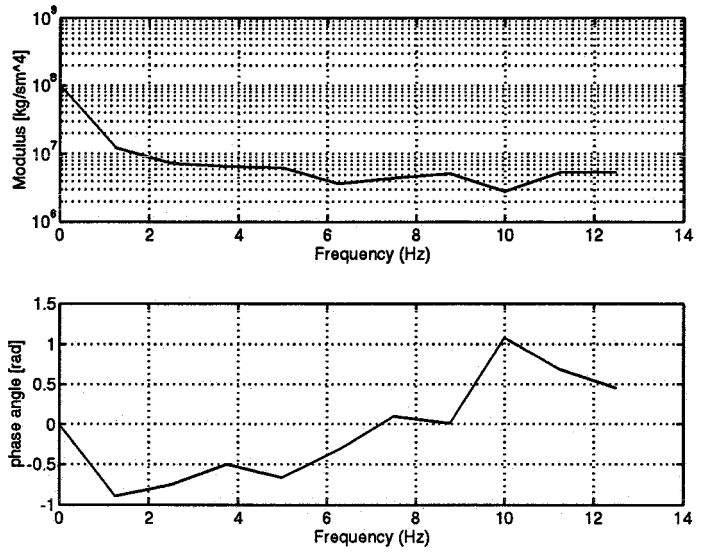

Figure 2.1: *Input impedance for the ascending aorta, from [Mil89].*

2.3.4 Impedance in man and dog

Impedance in man: Simultaneously measured pressure and flow in man have been recorded at relatively few sites in the arterial system since it requires surgical exposure of blood vessels. Most measurements determining input impedance in humans apply to the ascending aorta (input impedance of the arterial system) and femoral artery. Input impedance of the arterial system (aorta ascendens) is for example given by [Mil89, page 158], see figure 2.1, who also presented moduli and phase angles for each pressure and flow harmonic.

Input impedance for other arteries in man (renal, innominate, illiac and subclavian arteries, ascending aorta, aortic arch, descending aorta (T7 and T10) and abdominal aorta) are presented in [Mil70]. The presented input impedance data for these blood vessels were determined in terms of blood pressure and velocity recorded in patients aging from 24 to 60 years old. Conversion of this input impedance data into input impedance in terms of pressure and flow can be done by dividing the modulus of input impedance with the average cross-sectional area of the blood vessel. The quantity input impedance can not be used for the coronary arteries because coronary impedance is time-dependent and non-linear (see [Klo85]).

Impedance in dogs: Determination of input impedance has been performed more often in dogs than in humans. O'Rourke [Rou67] determined input impedance in a 21 kg anesthetized dog for the ascending aorta, upper descending thoracic aorta, abdominal aorta, brachiocephalic, carotid and femoral artery. Attinger [Att66] determined input impedance in twelve anesthetized dogs for the ascending aorta, descending aorta, abdominal aorta, superior mesenteric artery, carotid artery and femoral artery. The remark made on the coronary circulation of man also applies to the coronary circulation of dogs.

Input impedance determined in dogs can be scaled to human values using the dependance of the flow rate on body weight. Measurements limited to man and dog suggest that the cardiac output flow is proportional to the square root of the body weight. But in studies that include

a great variety of species an almost linear relationship is found between flow and body weight. This last relationship seems quite convincing [Mil83] and is used in this study.

2.4 A model for the terminal load of an artery

To describe pressure-flow relationships in arterial segments it is necessary to obtain a model for the terminal load. The earliest mathematical analogy of the circulatory system is the *Windkessel model* of Otto Frank (1899), and can thus be seen as a model for the input impedance of the arterial system as a whole. He suggested to represent the aorta and its major branches by an elastic air-chamber with uniform pressure and an internal volume that is linearily proportional to this pressure. He assumed that the rest of the circulatory system can be replaced by a fluid resistance. The name of this model is the German word for air-chamber. Later the original concept of the Windkessel was changed by introducing a fluid inertia element and a peripheral resistance, the latter representing the fluid resistance of the peripheral beds, see figure 2.2. Westerhof [Wes71] for example made a hydraulical model as a load for the heart based on this

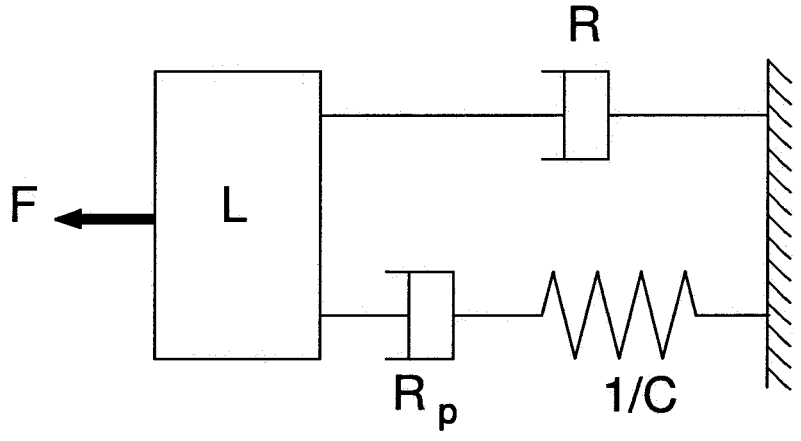

Figure 2.2: *A mechanical representation of the four-element Windkessel model. R_p represents the peripheral resistance, C is the compliance, L is an inertance and R represents the fluid resistance. F is the driving force (pressure).*

four-element Windkessel model. His model consists of three elements, a peripheral resistance, compliance and a resistance describing the characteristic impedance of the aorta and which can be treated as a combination of a fluid resistance and inertance.

The transfer function for the four-element Windkessel model, which will be reffered to as the *terminal impedance*, can be written as:

$$Z_{\text{term}}(j\omega) = \frac{(j\omega)^2 LCR_p + j\omega(L + CRR_p) + R + R_p}{1 + j\omega CR_p} \tag{2.35}$$

Such a four-element Windkessel model can also be used for the terminal load of a part of the arterial system, e.g. for the descending and abdominal aorta, renal and carotid artery. This

can be shown by employing the following approach: The terminal impedance for an artery can be calculated when the input impedance of the artery and the characteristics of the artery are known. The input impedance for the artery is known from literature [Mil70, Mil89]. The artery itself can be described by the longitudinal impedance in equation (2.28) multiplied by the length of the arterial segment, and the volume compliance of the segment. Physiological parameters (e.g. Poiseuille resistance, volume compliance, internal radius of the segment) for several arterial segments of about 5 cm length are presented in [Wes69]. The input impedance of the model for the harmonic component with angular frequency ω, Z_{im}, is known from literature and can be written in complex harmonic form in terms of the terminal impedance:

$$Z_{\text{im}}(\omega) = Z_{L_a} + \frac{Z_{\text{term}}}{j\omega C_a Z_{\text{term}} + 1} \tag{2.36}$$

where Z_{term} is given by equation (2.35), Z_{L_a} is the longitudinal impedance of the arterial segment and C_a is the compliance of the arterial segment. From equation (2.36) we can write the terminal impedance in the model in terms of the input impedance of the arterial segment and the properties describing the arterial segment:

$$Z_{\text{term}}(\omega) = \frac{Z_{L_a} - Z_{\text{im}}}{j\omega C_a (Z_{\text{im}} - Z_{L_a}) - 1} \tag{2.37}$$

The terminal impedance now found from equation (2.37) is fitted with the four model parameters for the terminal impedance (R, L, C and R_p) by using a least-squares method. From figures 2.3 it follows that the four-element Windkessel model gives a good description of the terminal load of the ascending aorta. The same holds for descending and abdominal aorta. The performance of the four-element Windkessel model as a terminal load for renal and carotid artery is slightly less for the first harmonics of the modulus of terminal impedance. This may be explained from the fact that the four-element Windkessel model treats the arterial system distal to the location for which the terminal impedance is defined, as purely elastic. This is a rather good assumption for the larger arteries. But more peripheral located arteries (like renal and carotid artery) show visco-elastic wall behavior.

The model parameters of the four-element Windkessel model for renal artery and aorta (ascending, thoracic and abdominal) are listed in table 2.2. It should be noted that the input impedance data described in [Mil70] are presented in terms of blood pressure and velocity. In order to convert input impedance in terms of pressure and flow, the modulus of input impedance is divided by the cross-sectional area of the blood vessel in question. Blood vessel radii were taken from [Wes69].

2.4.1 Influence of model parameters on the terminal impedance

The influence of the model parameters on terminal impedance is studied by changing the model parameters as listed in table 2.2 It can be concluded that:

- the inertance only affects the higher harmonics of modulus and phase of terminal impedance for ascending and descending aorta. For abdominal aorta and renal artery it does not have much effect on terminal impedance: terminal impedances for zero inertance and for an inertance of $1{\cdot}10^6$ kg/m^4 show almost no difference in modulus and phase of terminal impedance;

- the compliance mainly affects the modulus of terminal impedance for the first harmonics;

artery	parameters artery				parameters impedance			
	$R_a \cdot 10^5$	$L_a \cdot 10^5$	$C_a \cdot 10^{-11}$	int. radius	$R \cdot 10^5$	$L \cdot 10^5$	$C \cdot 10^{-11}$	$R_p \cdot 10^5$
ascending aorta	0.0327	0.31	53.4	1.5	43.7	0.53	730	986
descending aorta (T7)	0.397	1.74	59.7	1.0	30	2	150	3900
abdominal aorta (L1)	3.58	5.28	18.1	0.58	1600	*	50	15000
right renal artery	53.5	15.8	1.67	0.26	3200	*	15	11000

Table 2.2: *Model parameters for the arterial segment (subscript a) and the model parameters for the terminal impedance distal of the arterial segment. Resistance (R) is given in* $kgm^{-4}s^{-1}$, *inertance (L) is given in* kg/m^4 *and compliance (C) is given in* $m^4s^2kg^{-1}$. *An asterisk denotes that the corresponding parameter does not contribute much to the terminal impedance. The internal radius of the blood vessel is taken from [Wes69] and is given in centimeters.*

- the sum of the peripheral resistance and the entry resistance must equal the vascular resistance of the blood vessel. Therefore a change of about 5% in either the entry or peripheral resistance leads to a significant change in terminal impedance (which is mainly a consequence of the large influence of the entry resistance on the terminal impedance).

2.5 Reflections

The model derived for describing physiological pressure-flow relations in arteries (distensible tubes) can be further improved by taking reflections into account. Reflections will occur at the transition of the distensible tube and the terminal load. This transition can be considered as a discrete transition, i.e. the length of the transition is small as compared to the wavelength of the waves, so that there is no difference in pressure or flow between both ends of the transition. Consider a tube of length L which is terminated at $x = L$ with a terminal impedance Z_{term}. The pressure and flow in the tube are a sum of a forward travelling pressure and flow wave, respectively p_i^+ and Q_i^+, and a backward travelling wave, respectively p_i^- and Q_i^-. The transmitted pressure and flow wave are represented by p_t and Q_t. Continuity of pressure and flow at the transition located at $x = L$ can be expressed as:

$$p_i^+(\omega, L, t) + p_i^-(\omega, L, t) = p_t(\omega, L, t) \tag{2.38}$$

$$Q_i^+(\omega, L, t) + Q_i^-(\omega, L, t) = Q_t(\omega, L, t) \tag{2.39}$$

A relation for the reflection coefficient at $x = L$ can be obtained by using the concept of characteristic impedance. An expression for the characteristic impedance of a distensible tube can be obtained by substituting equations (2.16)–(2.18) and (2.20) in equation (2.10):

$$Z_C(\omega) = \frac{\hat{p}}{\hat{Q}} = \frac{k(\omega)}{\omega C'(\omega)} \tag{2.40}$$

Normally characteristic impedance is defined for waves travelling in positive x-direction, i.e. $k > 0$, so $\hat{p}_i^+ = Z_C \hat{Q}_i^+$. For waves travelling in negative x-direction (reflected waves) the pressure amplitude is then given by $\hat{p}_i^- = -Z_C \hat{Q}_i^-$. The impedance distal to the transition is in this case given by the terminal impedance Z_{term} from equation (2.35). It relates the complex

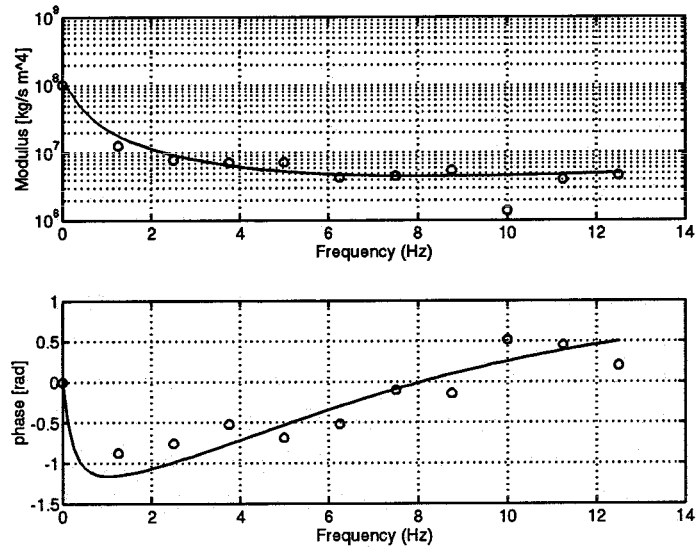

Figure 2.3: *Terminal impedance for the ascending aorta derived from [Mil89] (circles) and its fit (line). The model parameters are tabulated in table 2.2. The fundamental frequency is 1.25 Hz.*

amplitude of the transmitted pressure and flow waves: $\hat{p}_t = Z_{\text{term}}\hat{Q}_t$. Substituting Z_{term} and equation (2.40) into equations (2.38) and (2.39) yields an expression for the reflection coefficient Γ at $x = L$:

$$\Gamma = \frac{\hat{p}_i^-(\omega, L)}{\hat{p}_i^+(\omega, L)} = -\frac{\hat{Q}_i^-(\omega, L)}{\hat{Q}_i^+(\omega, L)} = \frac{Z_{\text{term}} - Z_C}{Z_{\text{term}} + Z_C} \tag{2.41}$$

We can now write the momentaneous flow (pressure) wave in the tube as a sum of the forward and backward travelling flow (pressure) waves and the reflection coefficient Γ. The forward travelling flow wave in the tube can be written as $Q_i^+ = \hat{Q}_i^+(\omega, 0)e^{i(\omega t - kx)}$ and the backward travelling flow wave $Q_i^- = \hat{Q}_i^-(\omega, 0)e^{i(\omega t + kx)}$. The complex amplitude of the momentaneous flow wave in the tube, $\hat{Q}_i$, is the sum of the complex amplitudes of forward and backward travelling flow waves. With some manipulation of terms this gives for $\hat{Q}_i$:

$$\hat{Q}_i = \hat{Q}_{i_o}^+ e^{-ik(x-L)}e^{-ikL} + \hat{Q}_{i_o}^- e^{ik(x-L)}e^{ikL} \tag{2.42}$$

where $\hat{Q}_{i_o}^+$ and $\hat{Q}_{i_o}^-$ are the complex amplitudes of the forward respectively backward travelling flow wave at $x = 0$. Using the definition of the reflection coefficient, $\hat{Q}_i$ can be written as:

$$\hat{Q}_i = \hat{Q}_{i_o}^+ e^{-ikL}\left\{e^{-ik(x-L)} - \Gamma e^{ik(x-L)}\right\} \tag{2.43}$$

Manipulation with the e^{-ikx}-term finally yields:

$$\hat{Q}_i = \hat{Q}_{i_o}^+ e^{-ikx}\left\{1 - \Gamma e^{2ik(x-L)}\right\} \tag{2.44}$$

The complex amplitudes of the forward travelling flow wave, $\hat{Q}_{i_o}^+$, can be calculated when the complex amplitudes of the momentaneous flow at $x = 0$ are known, with setting x to zero in the

equation above. A similar expression for the complex amplitude of the momentaneous pressure wave in the tube $\hat{p}_i$ can be derived following the approach above. This yields:

$$\hat{p}_i = \hat{p}_{i_o}^+ e^{-ikx} \left\{ 1 + \Gamma e^{2ik(x-L)} \right\} \tag{2.45}$$

The impedance in the tube can now be written as:

$$Z = \frac{\hat{p}_i}{\hat{Q}_i} = Z_C \left\{ \frac{1 + \Gamma e^{2ik(x-L)}}{1 - \Gamma e^{2ik(x-L)}} \right\} \tag{2.46}$$

with $Z_C = \hat{p}_{i_o}^+ / \hat{Q}_{i_o}^+$.

In chapter 4 the equations derived in this chapter will be used to compare experimental data with results obtained by the wave propagation model.

Chapter 3

Materials and methods

This chapter describes measurements of velocity in and wall displacement of a distensible tube under physiological pressure-flow conditions using laser-Doppler and ultrasound techniques. The measurements have been conducted in close cooperation with the University of Limburg, department of biophysics, where the ultrasound equipment has been developed. The purpose of these experiments is to compare laser-Doppler and ultrasound techniques for measuring velocity profiles in and distension of the distensible tube. Furthermore impedance is estimated from simultaneously measured distension of and center-line velocity in the tube using ultrasound techniques. In this way the ultrasound system is tested for determining impedance that can be measured easily in clinical practice.

3.1 Experimental setup

The experimental setup is depicted schematically in figure 3.1. The setup consists of a water filled tank in which a silicon rubber (Sylgard 184) tube is suspended. The unconstrained tube has a length of 50 cm, wall thickness of 1 mm and inner diameter of 18 mm. The tube in the tank is prestrained to 54.5 cm. The flow conditions in the setup have been scaled 1:1, which corresponds to flow conditions in the thoracic aorta of man. In order to create physiological pressure-flow relations in the distensible tube, the tube is terminated with the hydraulic load described in appendix B. This hydraulic load is adjusted to parameters which create a terminal impedance that is characteristic for the thoracic aorta:

- entry resistance $\pm\ 3{\cdot}10^{6}$ $\mathrm{kgm^{-4}s^{-1}}$;
- peripheral resistance $\pm\ 3{\cdot}10^{8}$ $\mathrm{kgm^{-4}s^{-1}}$;
- compliance of $\pm\ 1.5{\cdot}10^{-9}$ $\mathrm{m^{2}s^{2}kg^{-1}}$;
- inertance of $\pm\ 2{\cdot}10^{5}$ $\mathrm{kg\ m^{-4}}$.

The setup is filled with a water–glycerol mixture with a viscosity equal to that of blood (ν = $3.4{\cdot}10^{-6}$ $\mathrm{m^{2}s^{-1}}$). The density of the water in the tank is matched to the density of the water–glycerol mixture with salt, so that the elastic tube is freely suspended in the tank. The approximately 1.5 m long glass pipe, diameter 18 mm, provides a fully developed velocity profile at the entrance of the distensible tube.

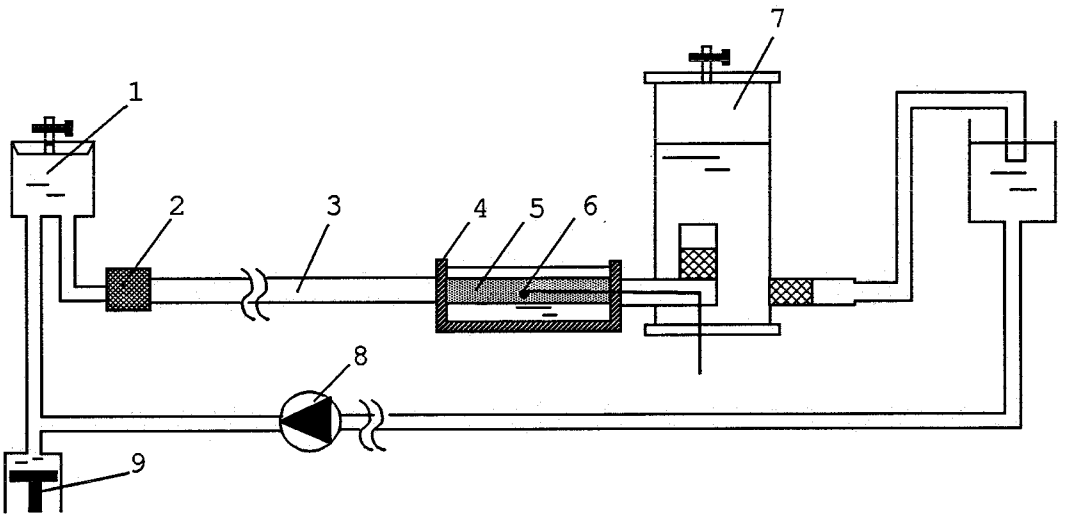

Figure 3.1: *Experimental setup in which velocity profiles and wall displacement of a distensible tube are measured. Legend: 1: tank, 2: flowmeter, 3: 1.5 m long glass pipe, 4: tank, 5: distensible tube, 6: catheter-tip pressure transducer, 7: hydraulic load, 8: stationary pump, 9: piston pump.*

3.2 Instrumentation

The flow is generated with two pumps: a stationary pump (VERDER) which generates mean flow, and a piston pump (Superpump, Vivitro Systems Inc.) which generates the harmonic components of the flow pulse. The flow at the entrance of the setup is measured with an electromagnetic flowmeter (SKALAR instruments).

The pressure in the distensible tube is measured with a mikro-tip catheter pressure transducer (type PC350, Millar Instruments Inc., Houston, Texas USA) which is connected to an amplifier (PEEKEL). The transducer was calibrated in a range from 0 to 20 kPa using a mercury filled U-tube.

The laser-Doppler anemometer (laser, optics, diode detector) is attached to a 3-D traversing system. Positions are measured with a Heidenhain positioning system. The laser-Doppler system is configured in the reference beam mode. A He-Ne laser is used with a power of 5 mW and a wavelength of 632.8 nm (Spectra Physics). The dimensions of the measurement volume are: 330 μm in radial direction and 80 μm in both vertical and axial direction. More information on the laser-Doppler anemometer and vibrometer system is given in appendix C.

The diode detector current from the LDA system is first processed in the tracker unit. The tracker unit (DISA 55N12) determines the Doppler frequency from the diode detector current and converts it into analog voltage. This analog voltage is proportional to the Doppler frequency. The tracker unit is calibrated by applying a known frequency and reading out analog voltage.

The tracker unit output signal, analog voltage from pressure transducer, flow meter and positioning system are acquired with a data-acquisition program written in LABVIEW in connection with a AT-MIO-16-L9 data-acquisition card of National Instruments. The piston pump and the laser-Doppler traversing system are also controlled by this program.

The laser-Doppler and ultrasound techniques need seeding of small particles from which the laser light or ultrasound waves are scattered. However both methods require different kinds of seeding. In order to be able to measure with both techniques in the same fluid, the following approach was adopted: The seeding for ultrasound measurements was provided by micro-air bubbles (diameter approximately 12 μm) which were generated by injection of pressurized air in the tank located downstream the hydraulic load. The stationary pump chops the air bubbles into smaller ones and a clamp behind this pump generates a jet of micro bubbles. A little tank prevents the larger air bubbles from entering the distensible tube. For laser-Doppler velocity measurements the supply of pressurized air is stopped and seeding is provided by injecting small amounts (2–3 ml) of a suspension of oil in water into the setup.

Two ultrasound systems are used in the experiments, see figure 3.2: one system measures wall displacement and center-line velocity simultaneously in y-direction (vertical). The emission frequency of this ultrasound probe is 6.1 MHz. The other system measures wall displacement and velocity profile in r-direction (horizontal), with an emission frequency of 5 MHz. Both ultrasound probes measure at an angle of 66° with flow direction.

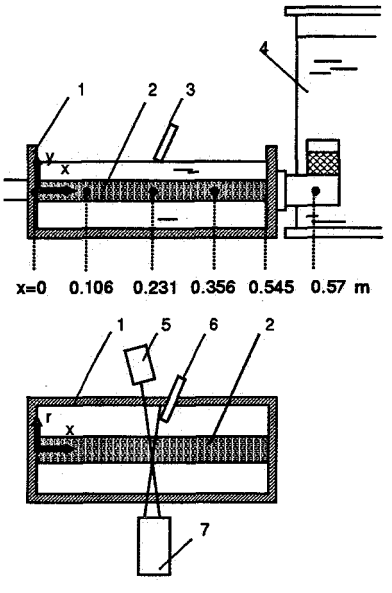

Figure 3.2: *Details of the measurement section. Black dots indicate the locations where pressure and/or distension and fluid velocity have been measured (upper). Top view of the setup (lower). Legend: 1: tank, 2: distensible tube, 3: ultrasound probe (vertical), 4: hydraulic terminal load, 5: diode detector, 6: ultrasound probe (horizontal), 7: laser and optics.*

3.3 Experimental methods

The flow pulse (frequency 1.0 Hz) is created from the complex amplitudes for the first ten harmonic components of an aorta flow pulse presented in [Mil89]. The amplitude of the flow pulse is scaled to the thoracic aorta with the ratio of the cross-sectional area of the aorta ascendens (internal radius 2.5 cm) and thoracic aorta (internal radius 0.9 cm).

Because of the different seeding requirements, laser-Doppler and ultrasound measurements of

distension and velocity can not be done simultaneously. Furthermore measurements of distension and velocity with the laser-Doppler equipment can not be conducted simultaneously: the vibrometer can not function without laser, laser optics and the signal processing unit that are used in the laser-Doppler anemometry. The following quantities have been measured at 10.6, 23.1 and 35.6 cm downstream the entrance of the tube (x=0):

- The static pressure-diameter relation has been measured. Pressure is quasi-statically increased by increasing the flow. The inner diameter of the tube is measured in horizontal direction with the laser. Positions are measured with the Heidenhain positioning system. With this relation the Young's modulus of the tube can be determined. Furthermore the offset of the distension measured with ultrasound and the laser-vibrometer can be determined using the static pressure-diameter relation.
- Dynamic pressure is measured ten times during eight cycles of the flow pulse at each location, with a sampling frequency of 128 Hz. Furthermore pressure is measured simultaneously with measurements of distension and velocity profiles.
- Velocity profiles have been measured with ultrasound techniques and laser-Doppler anemometry in order to compare both methods, and to determine flow in the tube (from integration of the velocity profile).
  - **Ultrasound:** velocity profiles have been measured in horizontal direction four times, each time during one flow cycle with a pulse repetition frequency of 6 kHz (distension is measured simultaneous with the same probe). Velocity is measured at 144 equidistant positions. Because of the large amount of data involved for measuring a velocity profile, velocity could be measured for not more than one second each time.
  - **Laser-Doppler anemometry:** Near the front wall of the tube the laser-Doppler system is traversed over 16 steps of 0.2 mm, next the system is traversed over 38 steps of 0.4 mm and near the back wall of the tube over 15 steps of 0.2 mm [1]. At every step, velocity (i.e. tracker voltage) and pressure have been measured simultaneously during 16 cycles with a samplefrequency of 128 Hz.
- Distension of the tube is measured with both ultrasound techniques and the laser-vibrometer in order to compare both methods. Using ultrasound techniques, distension is measured in horizontal and vertical direction. To avoid interaction of the two ultrasound systems, these measurements have been conducted apart from each other. Distension in vertical direction has been measured ten times with a pulse repetition frequency of 8 kHz during four seconds. Center-line velocity is measured simultaneously with the same probe, in order to determine impedance in terms of distension and center-line velocity. Distension in horizontal direction was measured four times (simultaneously with measurements of velocity profiles), each time during one flowcycle with a pulse repetition frequency of 6 kHz. Distension measured with laser-vibrometer is determined from measurements of front and back wall velocities. Both wall velocities have been measured separately during 32 cycles with a sampling frequency of 128 Hz.

In order to characterize the whole system (tube and hydraulic load) in terms of input impedance, pressure and flow have been measured ten times at the entrance of the distensible tube (x=0), each time during eight periods of the flow pulse with a sampling frequency of 128 Hz.

[1] Positions are divided by the refractive index of the water–glycerol mixture, to correct for the optical path length. The refractive index of the water–glycerol mixture is 1.384

Lastly the hydraulic terminal impedance was characterized in terms of input impedance. To measure flow at the entrance of the hydraulic terminal load, the tank with tube was removed from the setup. Pressure and flow at the entrance of the hydraulic terminal load were then measured ten times, each time over eight cycles.

3.4 Data processing

The flow at the entrance of the distensible tube and the pressure in the tube are determined from the calibration curves for flow meter and pressure transducer. The flow and pressure are ensemble averaged. The fluid and wall velocity measured with LDA and laser-vibrometer respectively are calculated from the calibration of the tracker unit. The fluid and wall velocity are then ensemble averaged. The flow in the distensible tube is determined from integration of the measured velocity profile. The distension of the tube measured with laser-vibrometer is determined from integration of the ensemble averaged wall velocity of back and front wall. Subtraction of front and back wall displacement gives the distension of the tube. The input impedance is determined from Fourier analysis of the ensemble averaged pressure and flow signals. The standard deviation for flow measured with the flow meter is $3{\cdot}10^{-7}$ m^3/s, and for pressure 70 Pa.

Chapter 4

Results

In this chapter, results from the experiments described in chapter 3 are shown. Measured pressure, flow, velocity profiles in and distension of the tube measured with laser-Doppler techniques are compared with the linear wave propagation model described in chapter 3. Ultrasound en laser-Doppler techniques are compared with eachother for measuring velocity profiles and distension. An alternative impedance based on distension and center-line velocity is determined and compared with theory.

4.1 Experiments versus model

In figures 4.1–4.3 experimental results are compared with the one-dimensional wave propagation model derived in chapter 2, for respectively 10.6, 23.1 and 35.6 cm downstream the entrance of the tube. Theoretical curves are shown as solid lines in all the figures. The **top left and right** figures show measured pressure and flow as dots. The flow is determined from integration of the velocity profile measured with laser-Doppler; **center left**: distension measured with ultrasound (dashed line) and laser-vibrometer (dots) in horizontal direction; **center right**: center-line velocity measured with ultrasound in vertical direction (dashed line) and determined from laser-Doppler velocity profiles (dots); **center**: velocity profiles measured with laser-Doppler anemometry (dots) shown for intervals of 16/128 seconds. The full length of such an interval corresponds with a velocity of 1 m/s; **bottom**: one half of the velocity profiles measured with ultrasound in horizontal direction (dots).

The marked dip in the pressure pulses show that reflections are present. Reflections occur at the transition of tube and hydraulic load. The reflection coefficient is determined from the characteristic impedance of the distensible tube and the input impedance of the hydraulic load, using equation (2.41) and (2.40). The wall thickness, Young's modulus and internal radius of the tube for mean pressure have been determined from the measured static pressure-diameter relation of the tube, using an expression for the Young's modulus and wall thickness of a thick-walled elastic tube [Sch94]. The Young's modulus was determined at $7.2 \cdot 10^5$ Pa and the wall thickness for mean pressure at 0.79 mm. The internal radius for mean pressure is determined at 1.06 cm. The compliance of the tube is calculated for a thin-walled elastic tube using equation (2.33) with Poisson's ratio (μ) set to 0.5. The modelparameters of the hydraulic load have been determined from a fit of the input impedance of the hydraulic load up to the six-th harmonic, see figure 4.4, based on the four-element Windkessel model. They are:

- entry resistance: $2.1 \cdot 10^7$ kgm^{4}s^{-1};

- inertance: $2.6 \cdot 10^5$ kgm^4;
- compliance: $1.0 \cdot 10^{-9}$ m^{4}s^{2}kg^{-1};
- peripheral resistance: $3.2 \cdot 10^8$ kgm^{4}s^{-1}.

The flow measured at the entrance of the distensible tube is used as input for the model.

4.1.1 Pressure and flow

The flow in the tube is determined from integration of the velocity profiles measured with laser-Doppler anemometry. Comparison of computed and measured flow shows that computed flow corresponds almost exactly with measured flow, see figures 4.1–4.3. The shape of the theoretical pressure wave mimics the shape of the measured pressure wave, only its mean value is about 10% higher than in the experiments, see figures 4.1–4.3. The phase velocity of measured pressure and flow waves is determined at 6.0 ms^{-1} while in the model it is 5.7 ms^{-1}. However, it should be noted that the model is sensitive to errors in some of the parameters that are used, such as Young's modulus and wall thickness of the distensible tube and the model parameters of the hydraulic load.

In figure 4.5 input impedance in the tube for positions x=0 cm and x=35.6 cm is shown. The influence of the inertia of the fluid in the tube is clear: the phase angle of input impedance becomes positive for lower frequencies towards the entrance of the distensible tube. This arises from the fact that the inertance of the fluid increases. It should be noted that for frequencies above 6 Hz the pressure amplitude is within the noise level.

4.1.2 Distension versus pressure

The compliance for purely elastic tube (equation (2.33)) has been used in the wave propagation model, therefore the distension is proportional to and in phase with pressure. Figures 4.1 – 4.3 show that distension measured with laser-vibrometer is proportional to and in phase with theoretical distension (and measured pressure). The assumption of a purely elastic tube is thus a correct one.

4.1.3 Velocity profiles

Velocity profiles have been computed using the Womersley equation for fluid flow in distensible tubes, without the assumption of axial constraint [Wom57]. This relation is similar to equation (A.12) except that the second term in the brackets is multiplied with an extra parameter that only slightly differs from unity. The pressure gradient was derived by differentiating the complex amplitude of the momentaneous pressure wave in the tube (equation (2.45)) with respect to the axial coordinate x. Velocities were computed for the first ten harmonics of the pressure gradient, plus a parabola representing the steady flow. Comparison of computed and measured velocity profiles for ultrasound and laser-Doppler measurements is shown in figures 4.1 – 4.3.

4.1.4 Alternative impedance

Impedance can be estimated from the relation between distension of the tube and center-line velocity in the tube. Distension and center-line velocity for large Womersley numbers and elastic tubes is almost linear with change in pressure and flow respectively. which is obvious from

figures 4.1 – 4.3. In order to compare this alternative impedance with impedance from measured pressure and flow, the distension, center-line velocity, pressure and flow must be normalized to values between 0 and 1. This alternative impedance for laser-Doppler measurements is similar to the computed alternative impedance and the impedance in terms of pressure and flow at 23.1 cm downstream the entrance of the tube, see figure 4.6.

4.2 Ultrasound versus Laser-Doppler techniques

This section compares ultrasound and laser-Doppler measurements of distension and velocity profiles. Furthermore an alternative impedance is determined in terms of normalized center-line velocity and normalized distension and is compared with the impedance determined from normalized pressure and flow.

4.2.1 Distension

Comparison of distension measured with ultrasound in both horizontal direction and vertical direction and laser-vibrometer shows that, see figure 4.7: (1) distension measured with ultrasound is not in phase with distension measured with laser-vibrometer, and (2) its absolute value of distension is lower than in the laser-vibrometer measurements. In figure 4.7 distension measured with ultrasound in vertical direction is shown too. It does not resemble distension determined from the laser-vibrometer: the motion of the tube in vertical direction is different from that in the horizontal direction. To obtain an offset value of diameter, distension was determined from the measured static pressure-diameter relation of the tube. The difference in absolute values of distension measured with both methods may be explained from the fact that distension of the tube measured with ultrasound was determined from the outer wall movements: reflections arising from the inner walls of the tube were too small to process, probably due to the attenuation of the ultrasound waves by the micro air bubbles.

Measurements of the distension of the tube were repeated at a later time with the laser-vibrometer and ultrasound techniques under similar conditions as described in chapter 3, but now without any seeding in order to determine distension from the inner wall movement. The results of these measurements show that (1) the distension of the tube measured with both laser-Doppler and ultrasound techniques are in phase with and proportional to pressure; (2) the distension measured with ultrasound techniques is of the same magnitude as measured with the laser-vibrometer.

4.2.2 Velocity profiles

A comparison between the velocity profiles measured with ultrasound and laser-Doppler techniques can only be made for one half of the velocity profiles: with ultrasound, only the first half of the velocity profile could be measured accurately enough. Probably the ultrasound waves are attenuated much by the micro air bubbles in the fluid. Velocity profiles measured with both ultrasound and laser-Doppler are shown in figures 4.1 – 4.3. The ultrasound velocity profiles are more flattened in the central region of the tube than the laser-Doppler velocity profiles. A three-dimensional plot of the velocity profiles measured with ultrasound and laser-Doppler techniques is given in figure 4.8.

4.2.3 Alternative impedance

In figure 4.9 the impedance is shown based on normalized center-line velocity and normalized distension determined from measurements with laser-Doppler and ultrasound techniques. The alternative impedance for the ultrasound measurements differs significantly from the laser-Doppler measurements, although alternative impedance measured in vertical direction is in better agreement with alternative impedance derived from laser-Doppler measurements than the one derived from measurements with ultrasound in horizontal direction. This difference can be explained from the large phase difference between the distension curves measured with ultrasound techniques and measured pressure curves.

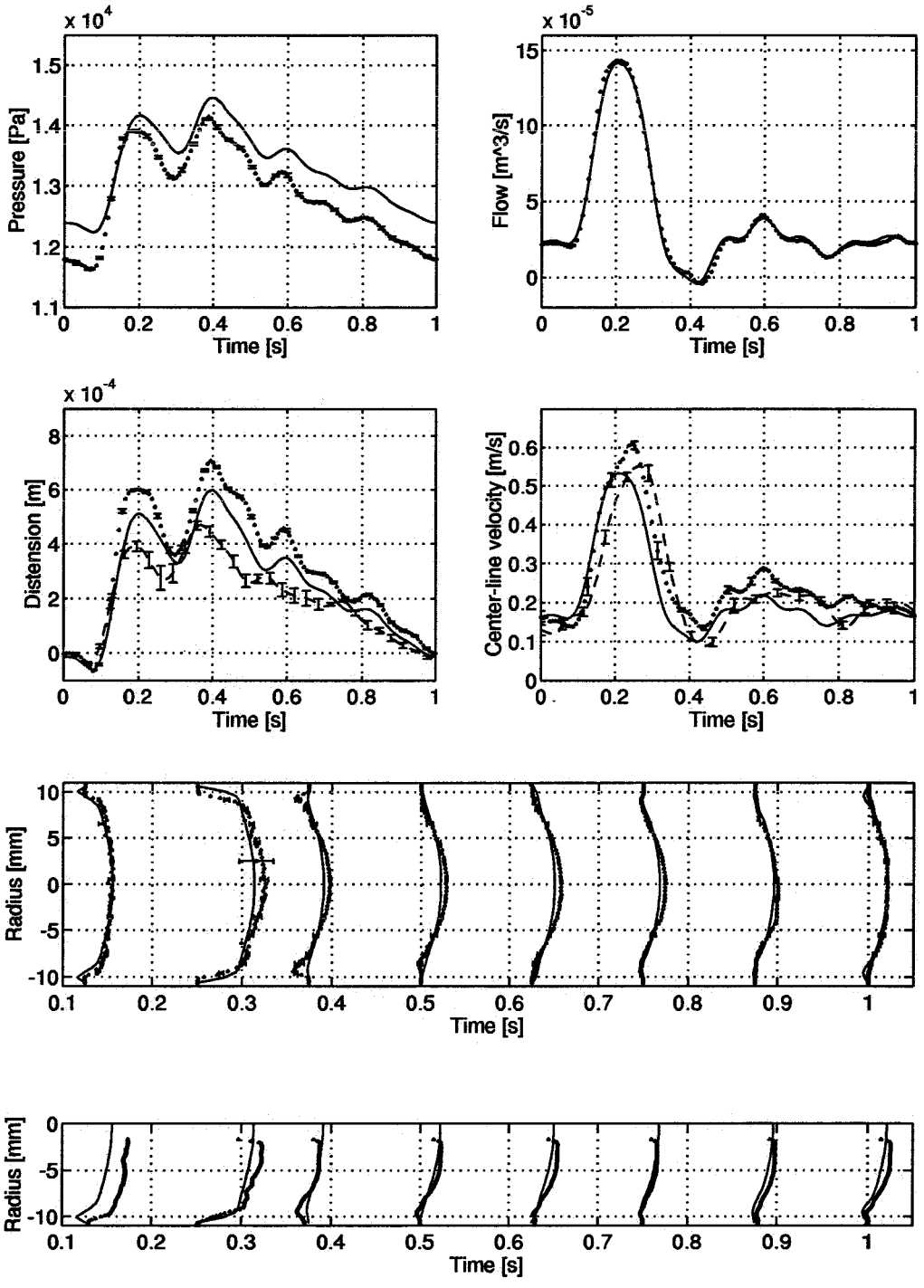

Figure 4.1: *Experimental results compared with theory for* **x=10.6 cm** *downstream the entrance of the tube. For explanation see text on page 22.*

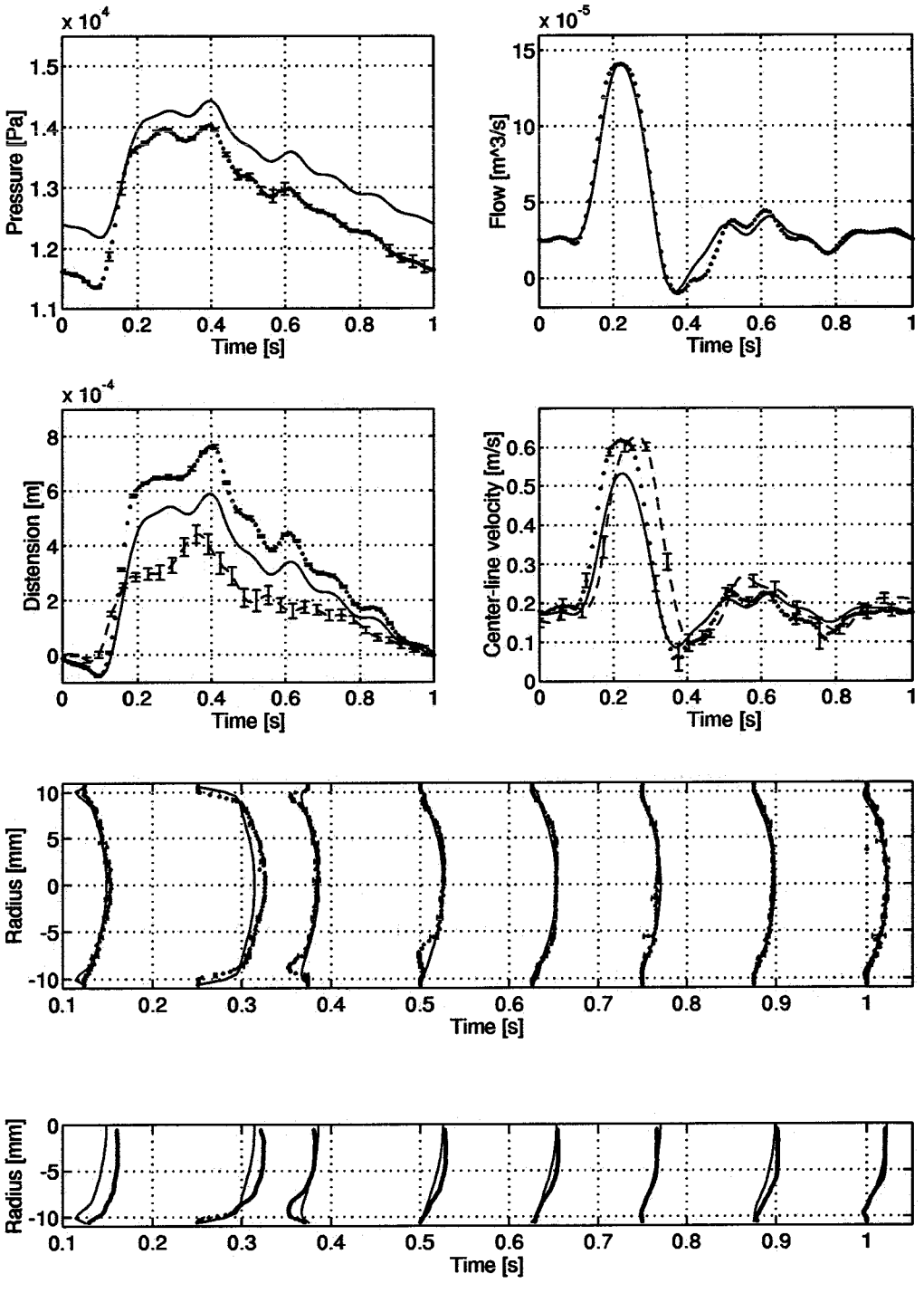

Figure 4.2: *Experimental results compared with theory for* **x=23.1 cm** *downstream the entrance of the tube. For explanation see text on page 22.*

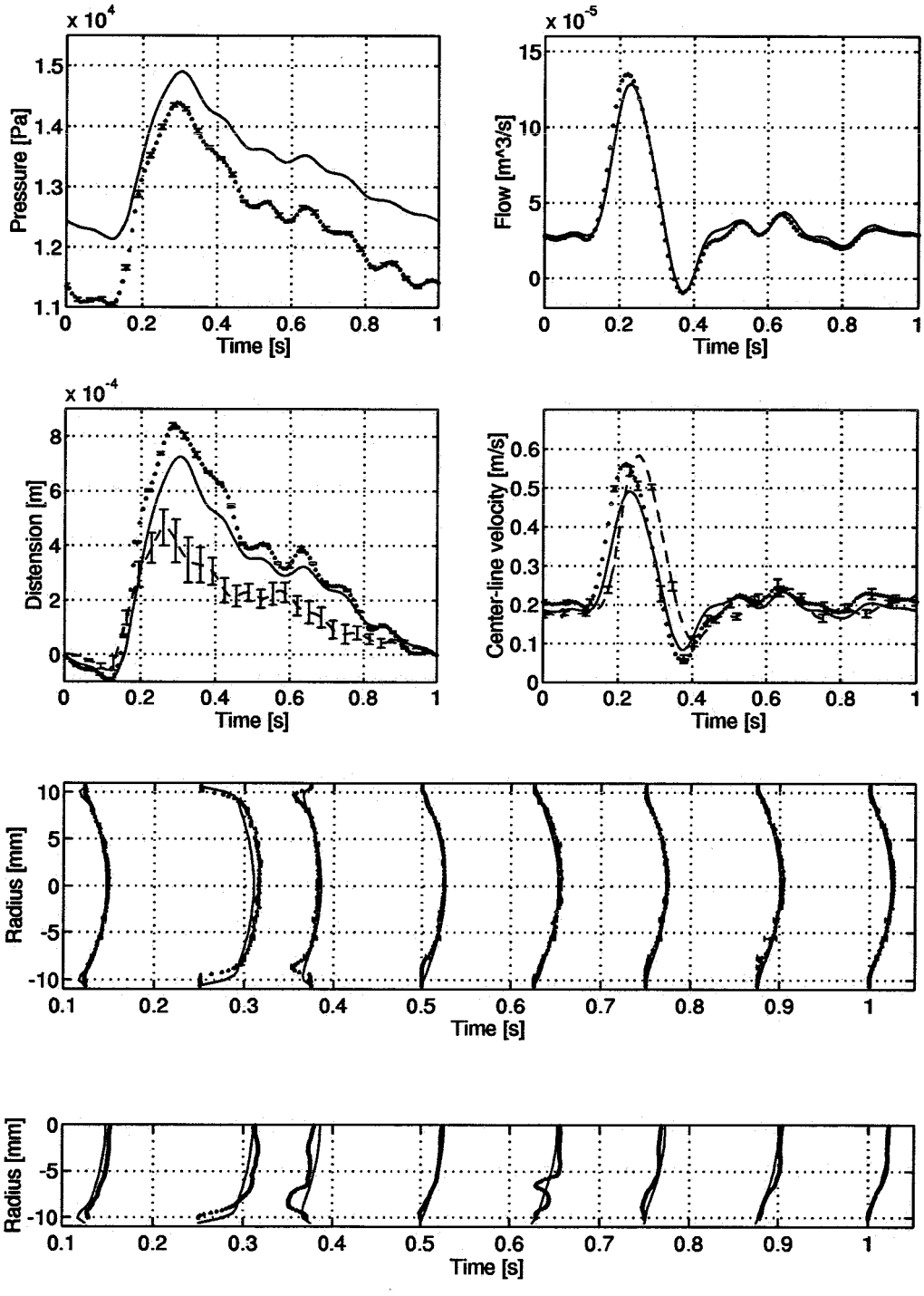

Figure 4.3: *Experimental results compared with theory for* **x=35.6 cm** *downstream the entrance of the tube. For explanation see text on page 22.*

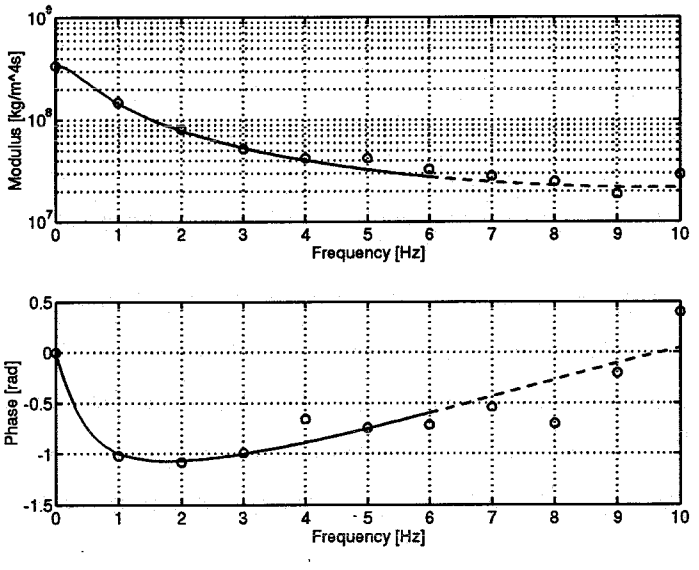

Figure 4.4: *Impedance of the hydraulic load, and its fit for frequencies up to 6 Hz.*

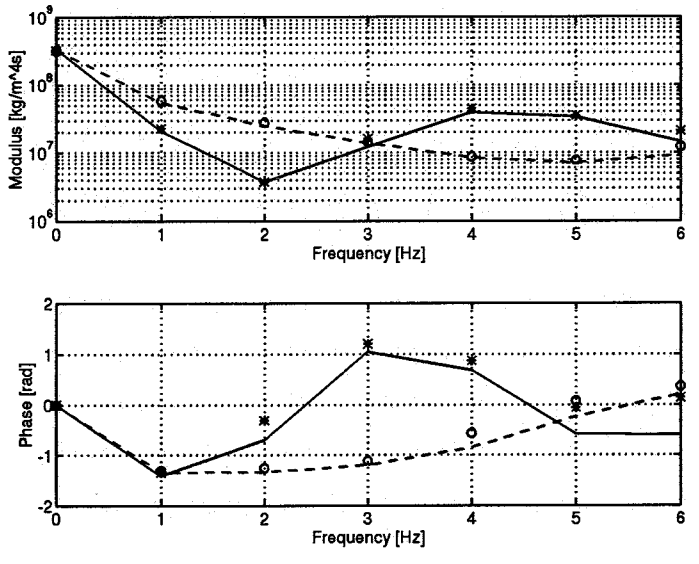

Figure 4.5: *Input impedance determined from measurements of pressure and flow at x=0 cm (*) and x=35.6 cm (o), compared with impedance determined from theoretical pressure and flow (dashed line for x=0, solid line for x=35.6 cm).*

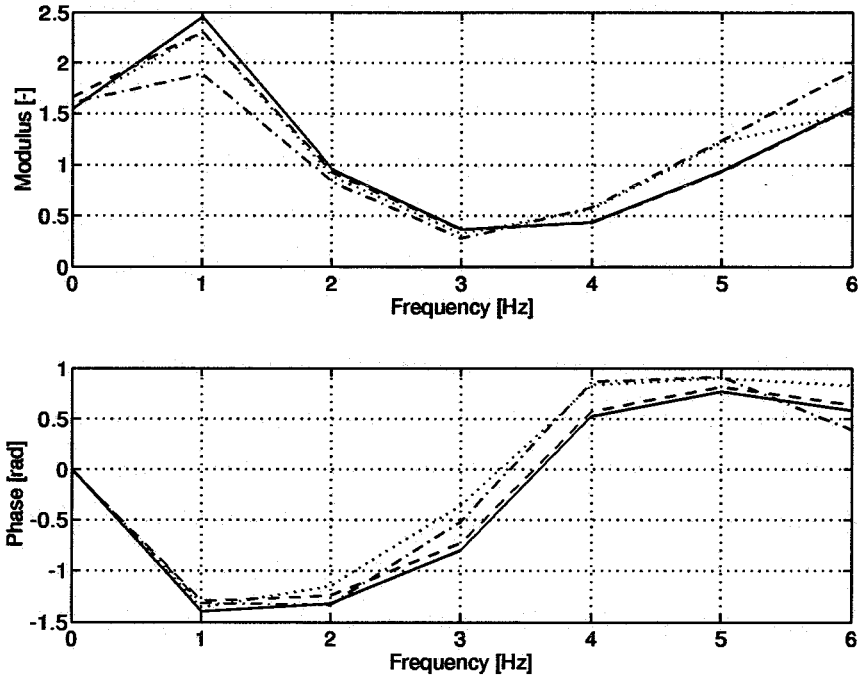

Figure 4.6: *Impedance determined from normalized measured (dotted line) and computed (solid line) flow and pressure, and alternative impedance determined for model (dashed line) and laser-Doppler measurements (dash-dot) at 23.1 cm downstream the entrance of the tube.*

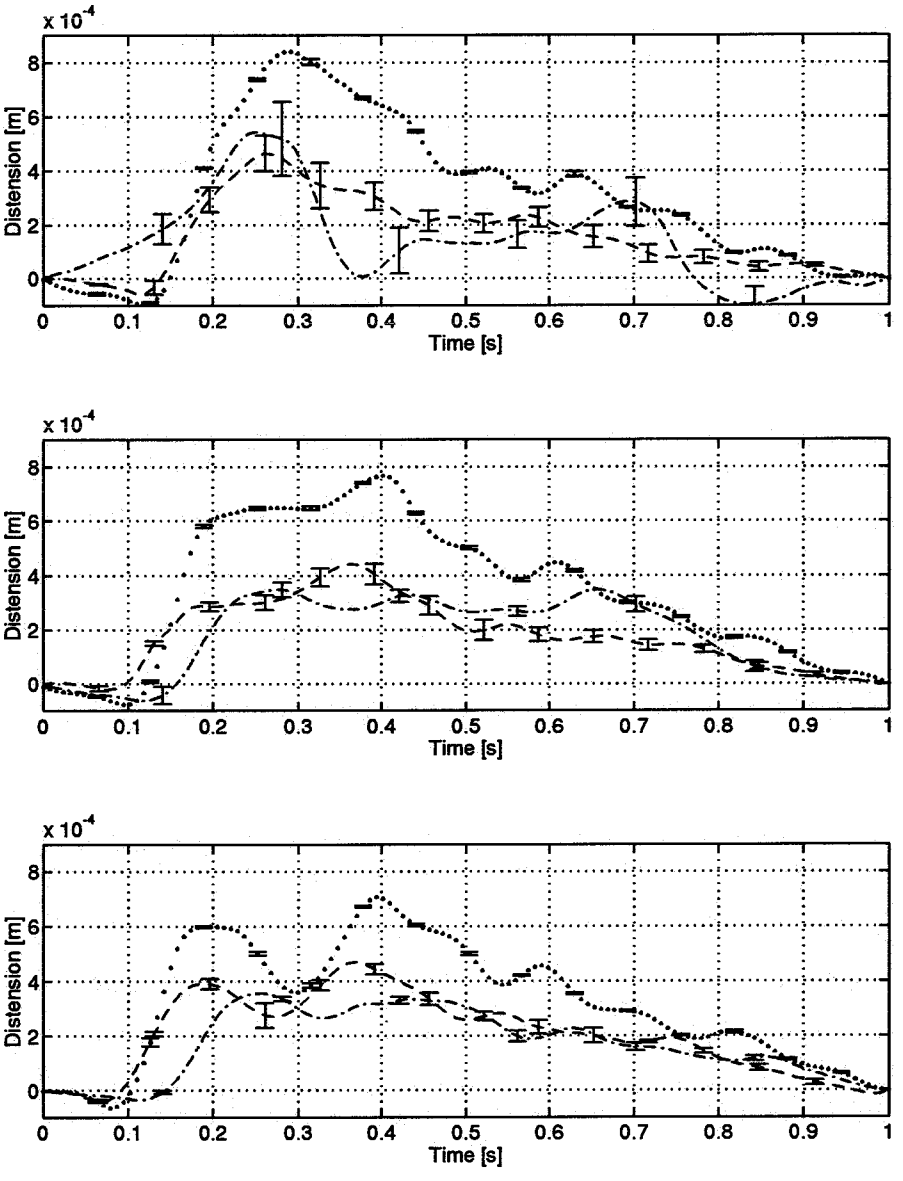

Figure 4.7: *Distensions measured with laser-vibrometer (dots), ultrasound in horizontal (dashed line) and vertical direction (dash-dot) at 35.6 cm (top), 23.1 cm (center) and 10.6 cm (bottom) from the entrance of the tube.*

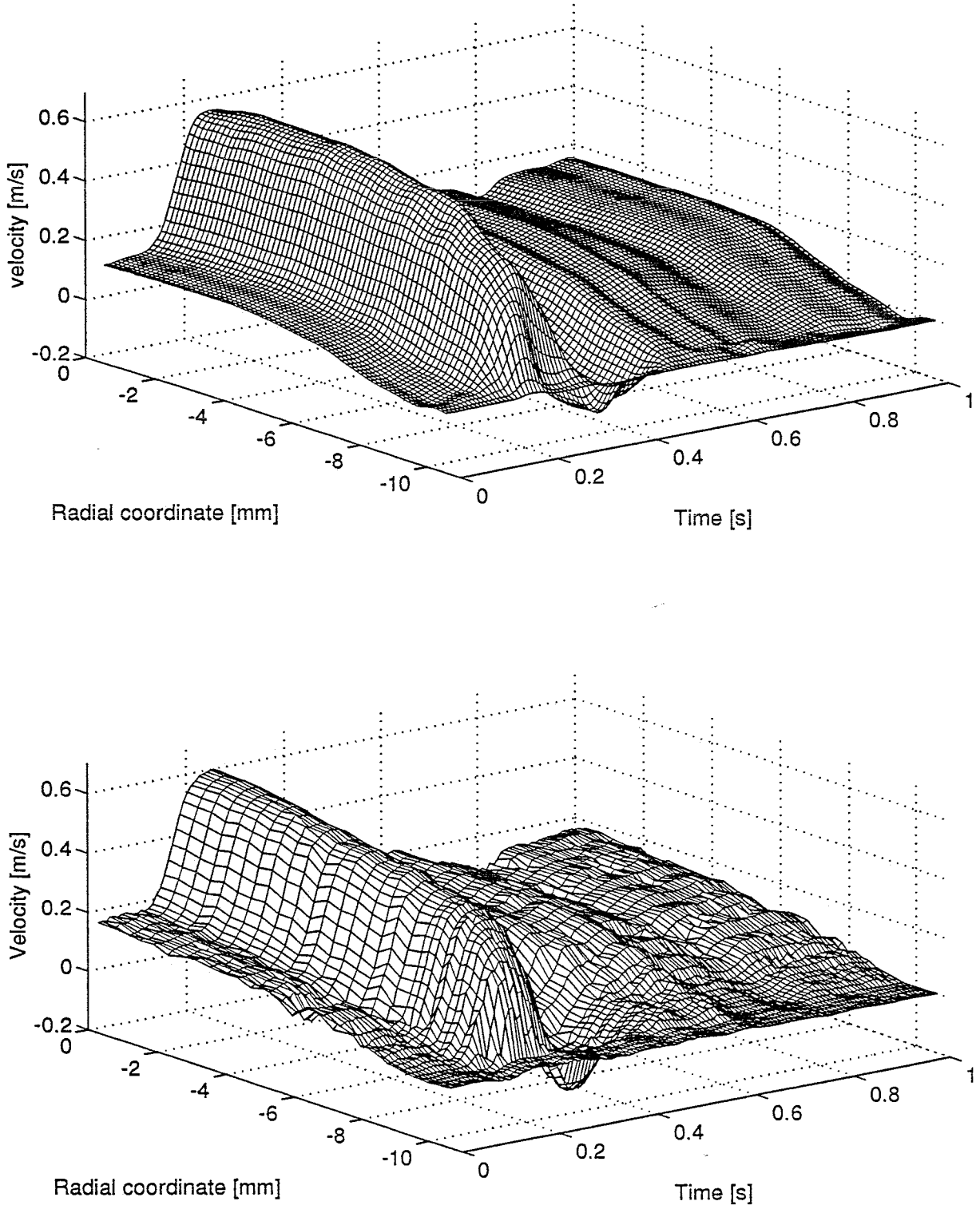

Figure 4.8: *3-D plot of velocity profiles measured with ultrasound (top figure) and laser-Doppler techniques (bottom figure), at 23.1 cm downstream the entrance of the distensible tube.*

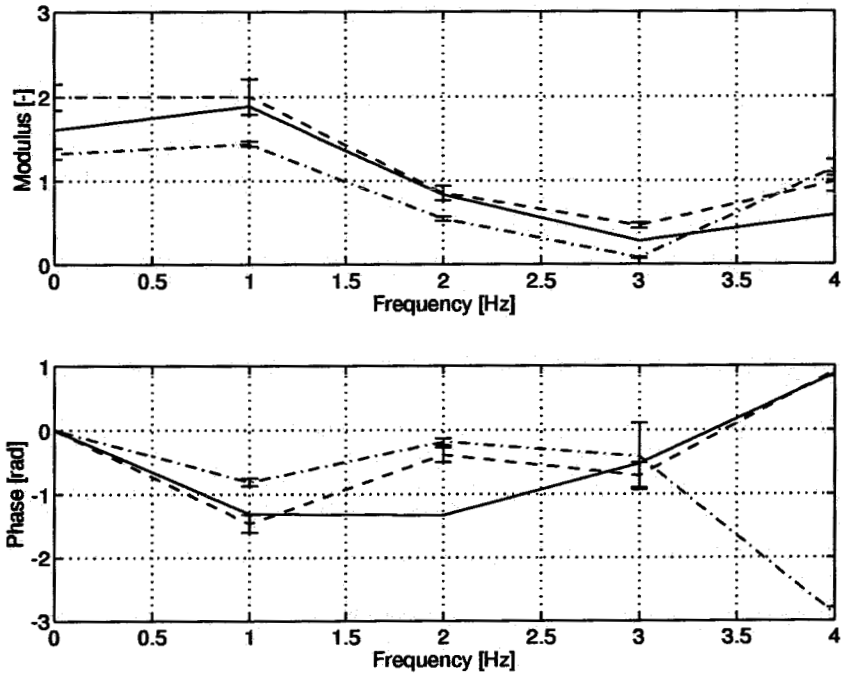

Figure 4.9: *Impedance for 23.1 cm downstream the entrance of the tube determined from normalized distension and center-line velocity measured with laser-Doppler (solid line), ultrasound in vertical direction (dashed line) and ultrasound in horizontal direction (dash-dot).*

Chapter 5

Discussion

One of the aims of this study was to design a hydraulic load with which physiological pressure-flow relationships in distensible tubes can be created. The input impedance of the hydraulic load developed in this study has the same characteristics as the impedance determined in man in the thoracic aorta. However, reflections are present in the system, so in fact physiological pressure-flow relations only exist nearby the point from which reflections occur (i.e. the transition from tube to hydraulic load). Although the hydraulic load in the experiments described in chapter 3 functions according to the four-element Windkessel model, tests of the hydraulic load in appendix B show that this is not always the case. This is probably caused by the frequency dependence of the resistance in the hydraulic load.

The linear wave propagation model for distensible tubes in which reflected waves are present gives a good description for measured flow, pressure and distension (measured with the laser-vibrometer), although there are some differences between model and measurements. The fact that computed pressure is about 10% higher than measured pressure can be explained from the fact that the steady-state resistance in the model is larger than measured. The computed center-line velocity is about 15% lower at peak systole than measured with both laser-Doppler and ultrasound techniques. This is probably caused by an overestimation of the inner diameter of the tube at mean pressure (which is detemined from the static pressure-diameter relation). Furthermore non-linearities in the experimental setup are present, such as a pressure dependent compliance. One could think of modelling the experimental setup in the time-domain, so that non-linearities can be introduced. One way of doing this is to partition the tube into a small number of segments, each segment represented by a resistance, inertance and compliance which are all pressure dependent.

The spatial resolution of the the laser-Doppler anemometer can be improved by changing the optics of the LDA-equipment in order to create a measurement volume with smaller dimensions (30μm in radial direction and 10μm in both other directions). This is necessary in future experiments when the experimental setup is scaled to flow conditions for a carotid artery. Then also wall shear rate can be determined accurately [Lou93].

Measurements of fluid velocity with ultrasound techniques can be improved by controlling the seeding requirements for ultrasound (concentration and size of the micro air bubbles). Comparison of data obtained from ultrasound and laser-Doppler measurements show that the ultrasound equipment provides valuable data for the determination of both wall displacement and velocity distribution in space and time. As a result the alternative impedance that can be derived from these data is accurate enough to obtain an impression of the impedance based on pressure and flow. However it should be noted that this relation between alternative impedance and

impedance based on pressure and flow only holds if the Womersley number of the flow is large enough ($\alpha \geq 8$; the Womersley number in the experiments described in this report is about 13) to ensure a linear relationship between center-line velocity and flow, and if the vessel wall shows purely elastic behavior. This will only be the case in larger arteries like the aorta and illiac arteries.

Bibliography

[Att66] E. Attinger, H. Sugawara, A. Navarro, A.Riccetto, and R. Martin. Pressure-flow relations in dog arteries. *Circulation Research*, 19: 230–245, 1966.

[Din81] U. Dinnar. *Cardiovascular fluid dynamics*, page 10. CRC Press, 1981.

[Disa] Laser-Doppler anemometry manual, DISA

[Fri93] Morton H. Friedman, Arteriosclerosis Research Using Vascular Flow Models: From 2-D Branches to Compliant Replicas, 1993. In: Noshir A. Langrana, Morton H. Friedman and Edward S.Grood, *1993 Bioengineering Conference*, volume 24, 1993

[Klo85] F.J. Klocke, R.E. Mates, J. John M. Canty, and A.K. Ellis. Pressure-flow relationships, controversial issues and probable implications. *Circulation Research*, 56: 310–323, 1985.

[Lou93] Zheng Lou, Wen-Jei Yang and Paul D.Stein. Errors in the estimation of arterial wall shear rates that result from curve fitting of velocity profiles. *Journal of Biomechanics*, volume 26, 1993.

[Mil70] C. Mills, I. Gabe, J. Gault, D. Mason, J. Ross, Jr, E. Braunwald, and J. Shillingford. Pressure-flow relationships and vascular impedance in man. *Cardiovascular Research*, 4: 405–417, 1970.

[Mil83] W.R. Milnor. *Hemodynamics.* Williams & Wilkins, Baltimore, 1^{nd} edition, 1983.

[Mil89] W.R. Milnor. *Hemodynamics.* Williams & Wilkins, Baltimore, 2^{nd} edition, 1989.

[Moe94] M.T.R. Moens. Validatie experimenten voor RTM simulaties met VIp, Report WFW no. 94.124.

[Rou67] M.F. O'Rourke. Pressure and flow waves in systemic arteries and the anatomical design of the arterial system. *Journal of Applied Physiology*, 23: 139–149, 1967.

[Sch94] F.A.O. Schepens. Deformatie van elastische buizen onder invloed van inwendige druk. Stageverslag, WFW rapport 94-043.

[Wes69] N. Westerhof, F. Bosman, C.J. de Vries, and A.Noordergraaf. Analog studies of the human systemic arterial tree. *Journal of Biomechanics*, 2: 121–143, 1969.

[Wes71] N. Westerhof, G. Elzinga, and P. Sipkema. An artificial arterial system for pumping hearts. *Journal of Applied Physiology*, 31: 776–781, 1971.

[Wes77] N. Westerhof, G. Elzinga, P. Sipkema, and G. van den Bos. *Quantitative Analysis of the Arterial System and Heart by Means of Pressure-Flow Relations*, chapter 11, pages 403–439. University Park Press, Baltimore London Tokyo, 1977.

[Wes79] N. Westerhof, P. Sipkema, and G. Elzinga. *Arterial Impedance*, chapter 3, pages 111–150. 1979.

[Wom57] J.R. Womersley. An elastic tube theory of pulse transmission and oscillatory flow in mammalian arteries. Technical report, Wright Air Development Centre TR56-614, 1957.

Appendix A

Pulsatile flow in rigid tubes

A.1 Longitudinal impedance

For a fully developed Newtonian flow in rigid tubes, the derivatives of the velocity in axial direction $\frac{\partial}{\partial x}$ and the velocity component in radial direction u_r are zero. Since the velocity in circumferential direction equals zero, the momentum equation and all derivatives in ϕ-direction are omitted. Now the Navier-Stokes equations reduce to:

$$\frac{\partial u_x}{\partial t} = -\frac{1}{\rho}\frac{\partial p}{\partial x} + \frac{\nu}{r}\frac{\partial}{\partial r}(r\frac{\partial u_x}{\partial r}) \tag{A.1}$$

The equation of motion can be written in dimensionless form by defining a dimensionless velocity ${u_x}' = u_x/U$. The coordinates can be made dimensionless using the tube radius, i.e. $r' = r/R_o$ and $x' = x/R_o$, the pressure can be scaled as $p' = p/\rho U^2$ and time can be made dimensionless using $t' = \omega t$. The equation of motion then becomes:

$$\alpha^2\frac{\partial {u_x}'}{\partial t'} = -Re\frac{\partial p'}{\partial x'} + \frac{1}{r'}\frac{\partial}{\partial r'}(r'\frac{\partial {u_x}'}{\partial r'}) \tag{A.2}$$

where Re is the Reynolds number given by

$$Re = \frac{R_o U}{\nu} \tag{A.3}$$

and α is the Womersley parameter:

$$\alpha = R_o\sqrt{\frac{\omega}{\nu}} \tag{A.4}$$

For a flow in a rigid tube the boundary condition $u(R_o, t) = 0$ is used. If we assume a harmonic pressure gradient and we search for harmonic solutions:

$$\frac{\partial p}{\partial x} = \frac{\partial \hat{p}}{\partial x}e^{i\omega t} \tag{A.5}$$

and

$$u_x = \hat{u}_x(r)e^{i\omega t} \tag{A.6}$$

substitution in equation (A.2) yields:

$$\nu\frac{\partial^2 \hat{u}_x(r)}{\partial r^2} + \frac{\nu}{r}\frac{\partial \hat{u}_x(r)}{\partial r} - i\omega\hat{u}_x(r) = \frac{1}{\rho}\frac{\partial \hat{p}}{\partial x} \tag{A.7}$$

Substitution of $s = i^{3/2}\alpha r/R_o$ in the homogeneous part of this equation gives the equation of Bessel for $n = 0$:

$$\frac{\partial^2 \hat{u}_x}{\partial s^2} + \frac{1}{s}\frac{\partial \hat{u}_x}{\partial s} + (1 - \frac{n^2}{s^2})\hat{u}_x = 0 \tag{A.8}$$

with the Bessel functions of the first kind as solution ($J_n(s)$). Together with the particular solution:

$$\hat{u}_x^p = \frac{i}{\rho\omega}\frac{\partial \hat{p}}{\partial x} \tag{A.9}$$

we have:

$$\hat{u}_x(s) = KJ_0(s) + \hat{u}_x^p \tag{A.10}$$

Using the boundary condition $\hat{u}_x(R_o) = 0$ then yields:

$$K = -\frac{\hat{u}_x^p}{J_0(\alpha i^{3/2})} \tag{A.11}$$

and finally we obtain the Womersley equation:

$$\hat{u}_x(r) = \frac{i}{\rho\omega}\frac{\partial \hat{p}}{\partial x}\left[1 - \frac{J_0(i^{3/2}\alpha r/R_o)}{J_0(i^{3/2}\alpha)}\right] \tag{A.12}$$

The mean flow Q can be derived using $sJ_0(s)ds = d(sJ_1(s))$ and $J_1(0) = 0$, which leads to:

$$Q = \int_0^{R_o} \hat{u}_x 2\pi r dr = i\frac{\pi {R_o}^2}{\rho\omega}[1 - F_{10}(\alpha)]\frac{\partial p}{\partial x} \tag{A.13}$$

The longitudinal impedance, $Z_L' = \frac{\partial p}{\partial x}/Q$, can now be written as:

$$Z_L' = \frac{i\alpha^2}{8}\frac{R'}{[1 - F_{10}(\alpha)]} \tag{A.14}$$

where R' is the Poiseuille resistance per unit length:

$$R' = \frac{8\eta}{\pi R_o^4} \tag{A.15}$$

A.2 Wall shear stress

Using the property of Bessel functions:

$$\frac{\partial J_o(s)}{\partial s} = -J_1(s) \tag{A.16}$$

and the definition:

$$F_{10}(\alpha) = \frac{2J_1(i^{3/2}\alpha)}{i^{3/2}\alpha J_0(i^{3/2}\alpha)} \tag{A.17}$$

the wall shear stress defined as:

$$\tau_w = -\eta\frac{\partial u_x}{\partial r}|_{r=R_o} \tag{A.18}$$

can be derived as:

$$\tau_w = \frac{-R_o}{2} F_{10}(\alpha) \frac{\partial p}{\partial x} = F_{10}(\alpha) \tau_w^p \tag{A.19}$$

with τ_w^p the wall shear stress for Poiseuille flow. Combining equations (A.13) and (A.19) finally yields:

$$\tau_w = \frac{R_o}{2A} i\omega\rho \frac{F_{10}(\alpha)}{1 - F_{10}(\alpha)} Q \tag{A.20}$$

with A the cross-sectional area of the tube.

Appendix B

Design and testing of a hydraulic load

Section B.1 describes the construction of a hydraulic equivalent of the four-element Windkessel model as a load for arterial segments. The experimental results of testing this hydraulic load are described in section B.2.

B.1 Design of a hydraulic load

This section describes the design of a hydraulic load based on the four-element model described in chapter 2. A hydraulic equivalent for each of the parameters in this model will be discussed in the following subsections.

B.1.1 A hydraulic resistance

The hydraulic resistors should meet some requirements:

- From chapter 2 it is clear that the hydraulic resistors have to be easily adjustable in a wide range of values: the entry resistance varies in a range from $1{\cdot}10^6$ to $4{\cdot}10^8$ $kgm^{-4}s^{-1}$, the peripheral resistance varies in a range of $8{\cdot}10^7$ to $1.6{\cdot}10^9$ $kgm^{-4}s^{-1}$;
- An ideal hydraulic resistance should be flow independant in the physiological arterial flow range (0 - 40 l/min), in order to have a time-independant hydraulic load. This is almost impossible and therefore some efforts should be made to keep the flow dependance of a hydraulic resistor as small as possible.

To realize a hydraulic resistance, reticulated filter foam was used (Uxem foam plastics, Valkenburg Z.H.). This is a polyester foam having a regular cell diameter and a regular open cell structure. Filter foam is available in different *porosities* (ϕ), i.e. the void volume fraction of the foam.

Characterisation of the foam

In order to have a well-defined resistor, the resistance of the foam as a function of the amount of foam, compression of the foam and flow should be determined. Resistance is defined as the ratio of pressure difference over the resistor and flow through the resistor. For fluid flow through

a porous medium for low Reynolds numbers the resistance of the porous medium is given by *Darcy's law* [Moe94]:

$$\frac{\Delta p}{Q} = -\frac{\eta}{kA}L \tag{B.1}$$

where k is the specific permeability, a term used for the conductivity of a porous medium with respect to Newtonian fluids, A is the cross-section of the sample, L is the length of the sample in the macroscopic flow direction and Δp is the pressure drop over the sample. The specific permeability is related to porosity by the relation [Moe94]:

$$k = \frac{\phi^3}{k_c A^2 (1-\phi)^2} \tag{B.2}$$

where k_c is the Kozeny constant.

For higher Reynolds numbers the Darcy equation has to be extended with an extra term [Moe94]:

$$\frac{\Delta p}{Q} = -\frac{\eta L}{kA} + bQL \tag{B.3}$$

with b an arbitrary constant. This relationship is often referred to as *Forchheimer's law.*

To characterize the resistance of the foam, the setup in figure B.1 was used. Cylindrical shaped foams with a diameter of 3 cm were used, having a porosity of 0.98. These foams were placed in a perspex holder (internal diameter 3 cm). The holder is placed between two constant head tanks which supply a pressure difference over the holder that is proportional to the vertical distance between the constant water levels in the tanks.

The resistance of the foam as a function of the amount of foam and compression was determined at three different flow rates (8, 16 and 24 ml/s). The flow rate is adjusted by changing the vertical positions of the constant head tanks and was measured with beaker and stopwatch. In order to determine the resistance of the foam itself, the resistance of the setup without any foam was measured too for the mentioned flow rates. The experiments show that the resistance of the foam for constant flow rate is proportional to the amount of foam, but varies with some 30% within the flow range of 8-24 ml/s, see figure B.2. The specific permeability is determined at $(2.8 \pm 0.4)\cdot 10^{-8}$ m^4 and the arbitrary constant in Forchheimer's law (b) is determined at $(2.3 \pm 0.4)\cdot 10^{12}$ kg/m^8. Furthermore the experiments show that the resistance of the foam for constant flow rate is inversely proportional to the compression factor, see figure B.3 and also varies with some 30% in the flow range of 8-24 ml/s.

These results point out that the fluid velocity through the foam under the specified conditions is too high to have a flow independent resistance (maximum Reynolds number, based on diameter, is 1100), so the Forchheimer law holds for the foam under these conditions. The fluid velocity through the foam must decrease in order to reduce the flow dependence of the resistance. This can be reached by increasing the cross-sectional area of the foam. On the other hand this means that more foam and/or more compression is needed to get the desired resistance values which leads to a inpracticable resistor.

B.1.2 A hydraulic compliance

The construction for the compliance is derived from Westerhof [Wes71]. Westerhof presented a three-element hydraulic model as a load for the arterial system. He constructed a compliance using an air reservoir. From the ideal gas law, $pV = RT$, and $C = \frac{dV}{dp}$ it follows that the

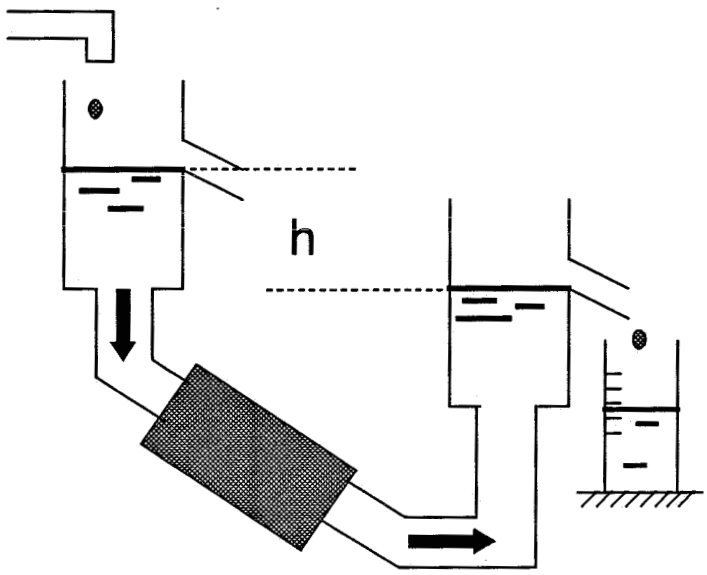

Figure B.1: *Experimental setup to determine the resistance of filter foam.*

compliance is described by the air volume and pressure above the fluid. Keeping in mind that an increase in fluid volume leads to a decrease in air volume, this yields:

$$C = \frac{V}{p} \tag{B.4}$$

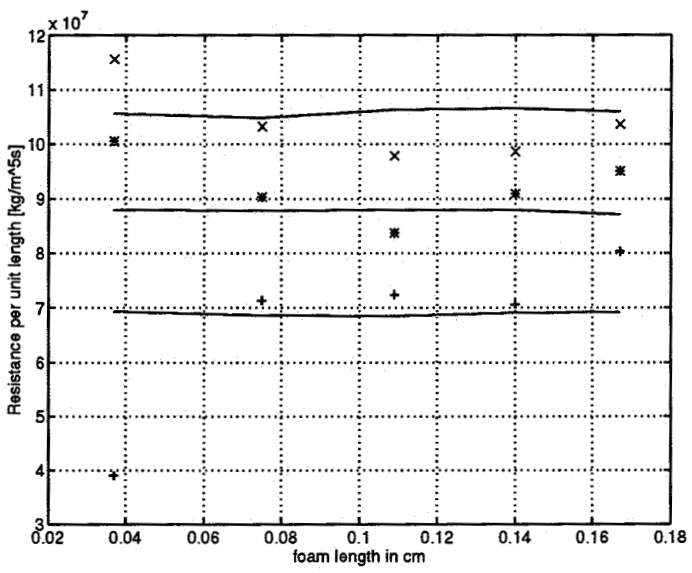

Figure B.2: *Resistance of foam as a function of the foam length for flows of 8 ml/s (+), 16 ml/s (*) and 24 ml/s (x). Lines show a fit based on Forchheimer's law.*

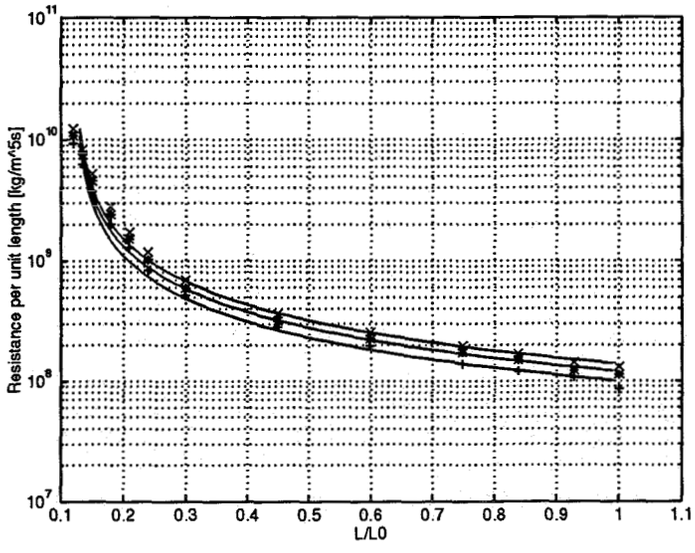

Figure B.3: *Compression of foam: resistance of foam as a function of the compression factor. The initial foam length used was 16.7 cm (L_0=16.7 cm).*

The reservoir is constructed as a perspex container with a diameter of 8 cm and a height of 35 cm. Its compliance can be adjusted by changing the fluid level in the air reservoir. The compliance may exhibit non-linearity when very small compliances are desired: for small compliances (small air volumes) the air volume changes in the reservoir as a result from arterial flow changes are relatively large with respect to the air volume in the reservoir.

B.1.3 A hydraulic inertance

For steady flow the inertance (L) of a rigid tube is proportional to the ratio of its length (l) and its cross-sectional area (A), $L = \rho l/A$. In order to create an inertance a set of six tubes can be used, having an internal diameter of 2.4 cm and varying length (from 1.5 to 10.5 cm). This corresponds to inertance values ranging from $3.3{\cdot}10^4$ kg/m^4 to $2.3{\cdot}10^5$ kg/m^4 (ρ taken as 1000 kg/m^3). One of these tubes is connected to the entrance of the hydraulic load and so it defines the entry inertance of the hydraulic load. The resistance of these tubes can be neglected with respect to the resistance of the foam.

B.1.4 The hydraulic load

When all hydraulical components are joined together the hydraulic load looks like figure B.4. The length of the entrance tube of the hydraulic load is 3 cm and its diameter is 3 cm (which corresponds to an inertance of $1.1{\cdot}\ 10^4$ kgm^{-4} for water). A water tank (measurement section) can be connected to the hydraulic load. A small tube connects the entrance tube of the hydraulic load with open air, to enable pressure measurements. The foam that is needed to form the entry resistance is placed on a gauze in the entrance tube of the hydraulic load. Another tube can be connected to the entry tube and serves as a foam holder and inertance. The entry resistance can be adjusted by screwing this tube further into the entry tube. The peripheral resistance can be

adjusted by compressing the foam with the adjustable holder. For both resistances cylindrically shaped polyester foam with porosity 0.98, is used, diameter of 3 cm. The compliance can be varied by adjusting the water level in the reservoir.

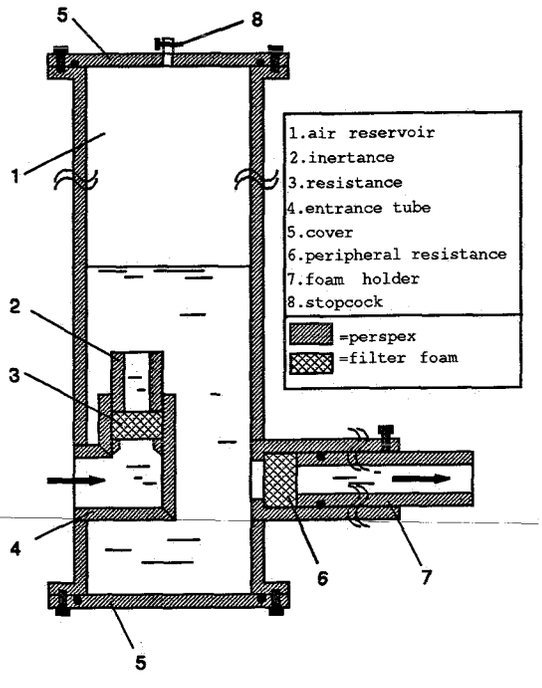

Figure B.4: *A cross-sectional drawing of the hydraulic load.*

B.2 Testing of the hydraulic load

The hydraulic load is tested in an expermental setup as shown in figure B.5. Stationary flow is generated with a stationary pump (VERDER). Sinusoidal flow is generated with a piston pump (Superpump, Vivitro Systems Inc. Cardiac Development Laboratory, Royal Jubilee Hospital, Victoria, B.C. Canada). Flow entering and exiting the hydraulic load is measured with electromagnetic blood flow meters (SKALAR instruments). Pressure is measured at the entrance of the hydraulic load with a mikro-tip catheter pressure transducer (type PC350, Millar Instruments Inc., Houston, Texas USA) and downstream the hydraulic load with a P10EZ piezo-electrical transducer. Both pressure transducers have been connected to an amplifier (PEEKEL instruments). The pressure transducers have been calibrated with a mercury filled U-tube.

The pressure and flow signals are acquired over eight periods of the flow signal with a data-acquisition program written in LABVIEW. This program also controls the piston pump. The recorded pressure and flow are ensemble averaged. The input impedance is determined from the Fourier coefficients of ensemble averaged pressure and flow.

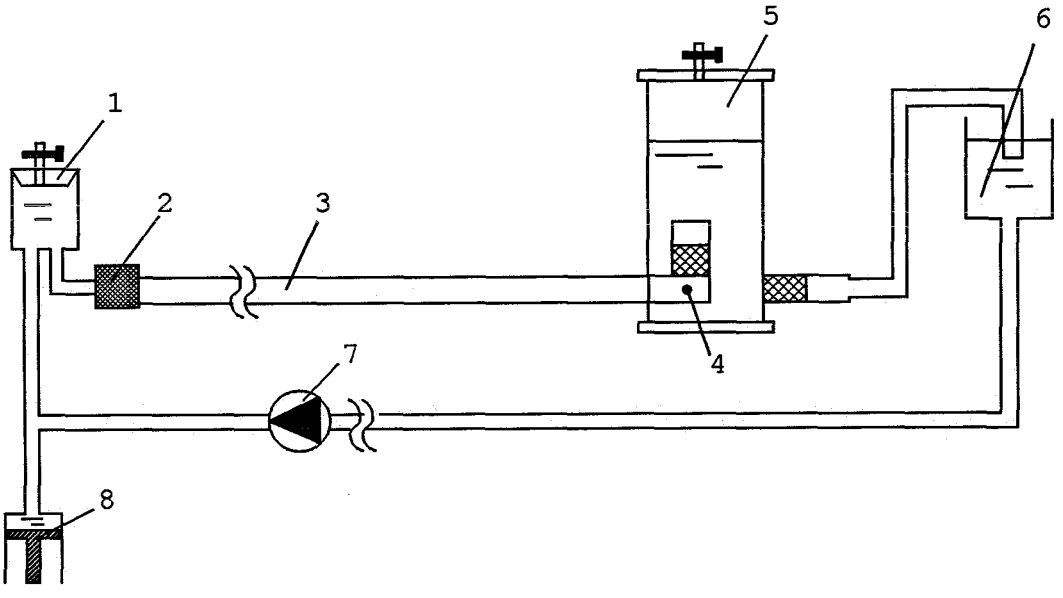

Figure B.5: *Experimental setup for testing the hydraulic load. 1: tank; 2: flow meter; 3: 1.5 m glass pipe; 4: pressure measurement point; 5: hydraulic load; 6: tank; 7: stationary pump; 8: piston pump.*

B.2.1 Testing of resistances

Both resistances have been tested by completely filling the air reservoir with water to avoid possible compliance effects. The pressure and flow are measured at the entrance and exit of the hydraulic load for different compression factors for the foam and for three different flow rates (8, 16 and 24 ml/s). The ratio of the measured pressure difference and entry flow gives the resistance of the setup between the pressure measurement points. In order to determine the resistance of the foam itself, the resistance of the hydraulic load without any foam in it was measured for the mentioned flow rates also. The results are similar to the experimental results described in subsection B.1.1.

B.2.2 Testing of compliance

When entry resistance and entry inertance of the hydraulic load can be neglected, the terminal impedance only depends on compliance and peripheral resistance:

$$Z_{\text{term}} = \frac{R_p}{1 + j\omega C R_p} \tag{B.5}$$

For $\omega C R_p \gg 1$, i.e. an infinite peripheral resistance, the phase angle of the terminal impedance is $-\frac{\pi}{2}$ radians and its modulus reduces to:

$$|Z| = \frac{1}{\omega C} \tag{B.6}$$

The setup is shut off behind the hydraulic load with a clamp in order to create an infinite peripheral resistance. The stationary pump is cut off from the setup. The compliance is adjusted

by changing the vertical position of the small constant head tank behind the hydraulic load and the stop cock that is connected to the air reservoir. The piston pump generates a sinusoidal signal with a preset frequency. Both flow and pressure at the entrance of the hydraulic load are measured over some periods of the flow signal and are ensemble averaged. This is done for several frequencies and for two different flow amplitudes: 1.5 l/min and 3.0 l/min. The compliance is now determined using equation (B.6). The modulus of pressure and flow for angular frequency ω, are determined using Fourier theory. This procedure is repeated for several compliances. The results are shown in figure B.6 and are compared with the theoretical compliance (calculated from equation (B.4)).

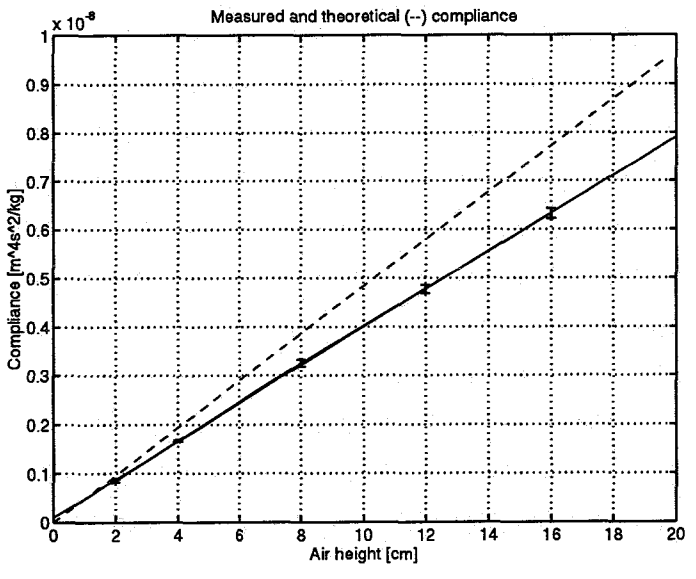

Figure B.6: *Comparison of measured (solid line) and theoretical compliance (dashed line) as a function of the height of the air column in the hydraulic load.*

B.2.3 Testing of inertance

The inertance can not be determined directly: the compliance can be made zero by completely filling the air reservoir with water, but there is always a a resistance of the hydraulical impedance (R_i) itself, which is in the order of $1{\cdot}10^7$ kg/m^{4}s. This resistance is much larger than the term $j\omega L$ ($L \leq 2 \cdot 10^5$ kgm^{-4}).

B.2.4 Testing overall behavior of hydraulic load

The hydraulic load is now tested for a combination of parameters: it is adjusted to a minimal entry resistance and inertance, and a peripheral resistance of $8{\cdot}10^7$ kgm^{-4}s^{-1}. Compliances are adjusted to values of $7.2{\cdot}10^{-9}$ and $3.5{\cdot}10^{-9}$ m^{4}s^{2}kg^{-1}. The input impedance of the hydraulic load has been determined for each compliance with a sinusoidal flow for various frequencies. The amplitude of the flow signal has been varied to test the (non-) linearity of the hydraulic (amplitudes of 8, 16 and 24 ml/s).

Results: For a compliance of $7.2{\cdot}10^{-9}$ $m^4s^2kg^{-1}$ the measurements show that the phase angle of the hydraulic load matches the theoretical phase angle (based on the settings of the hydraulic load) quite well. The modulus of the hydraulic load is somewhat higher than can be expected from the theoretical modelparameters, see figure B.7. It should be noted that the pressure amplitude for frequencies above 5 Hz cannot be measured accurately enough (the modulus of the impedance for the hydraulic load decreases with increasing frequency while the flow amplitude remains constant. This leads to a decrease of the pressure amplitude (the noise level for pressure is 80 Pa)). For smaller compliances the modulus of the terminal impedance is also

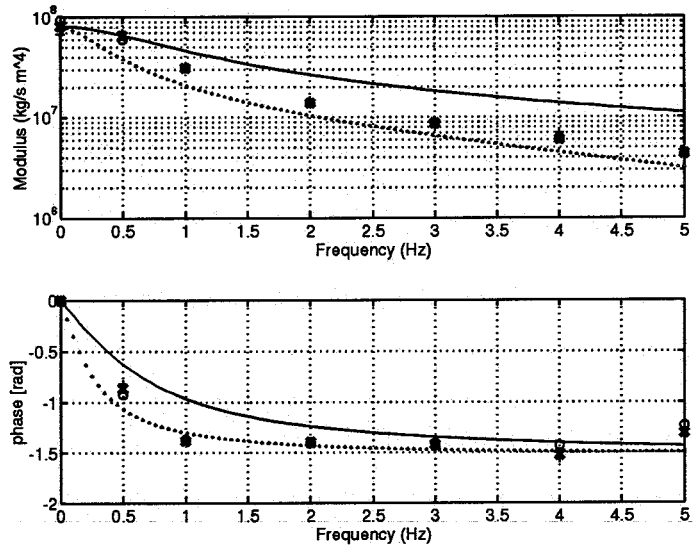

Figure B.7: *Impedance determined for flow amplitudes of 8 ml/s (+), 16 ml/s (x) and 24 ml/s (o); theoretical impedance (points) and impedance fit (line). Model parameters and theoretical parameters are listed in table B.1.*

Parameters	Impedance settings (theory)	Parameters from fit
C ($m^4s^2kg^{-1}$)	$7.2{\cdot}10^{-9}$	$2.8{\cdot}10^{-9}$
L (kg m^{-4})	$4{\cdot}10^4$	0
R (kg $m^{-4}s^{-1}$)	≈ 0	0
R_p (kg $m^{-4}s^{-1}$)	$8{\cdot}10^7$	$8.15{\cdot}10^7$

Table B.1: *Model parameters corresponding to the impedance in figure B.7.*

higher than can be expected from the settings of the hydraulic load. The phase angle matches the theoretical phase angle quite well for frequencies up to 3 Hz. But for higher frequencies the phase angle decreases to values lower than $-\frac{\pi}{2}$ radians, see figure B.8. An illustrative example of the (unexpected) phase behavior of the hydraulic load for higher harmonics is the following one: The hydraulic load is set to: $8{\cdot}10^7$ $kgm^{-4}s^{-1}$ for both resistances, the compliance is set to $7.2{\cdot}10^{-9}$ $m^4s^2kg^{-1}$ and minimal inertance. The phase angle of the impedance for the model of the hydraulic load with these settings shows a minimum for a frequency of 0.5 Hz (-0.35 rad)

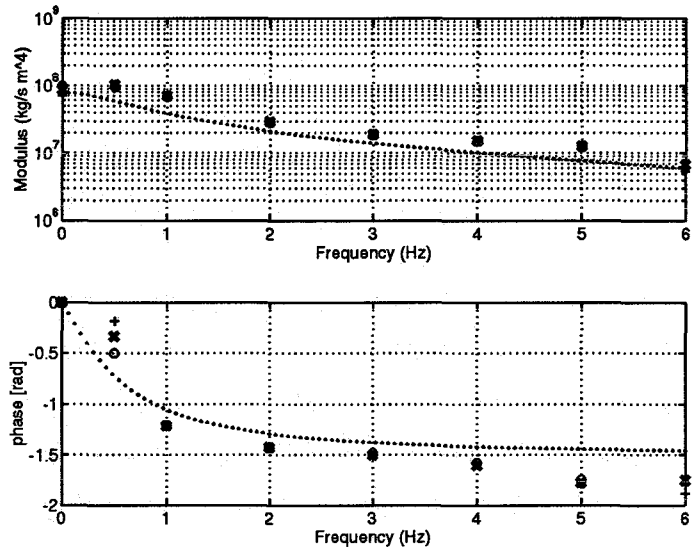

Figure B.8: *impedance determined for flow amplitudes of 8 ml/s (+), 16 ml/s (x) and 24 ml/s (o). The dotted line shows the impedance for the settings of the hydraulic load, which are: C= $3.5{\cdot}10^{-9}$ $m^4s^2kg^{-1}$, R_p=$8{\cdot}10^7$ kg $m^{-4}s^{-1}$ and minimal entry resistance and inertance.*

and then slowly goes to zero. Measurements show this behavior for frequencies up to 2 Hz. However, the phase angle for higher frequencies drops to $-\frac{\pi}{2}$ radians, see figure B.9.

Parameters	Impedance settings (theory)	Parameters from fit
C ($m^4s^2kg^{-1}$)	$7.2{\cdot}10^{-9}$	$3.3{\cdot}10^{-9}$
L (kg m^{-4})	$4{\cdot}10^4$	0
R (kg $m^{-4}s^{-1}$)	$8{\cdot}10^7$	$7.2{\cdot}10^8$
R_p (kg $m^{-4}s^{-1}$)	$8{\cdot}10^7$	$8.4{\cdot}10^7$

Table B.2: *Modelparameters corresponding to the impedance in figure B.9. Data up to 2 Hz are used in the fit only.*

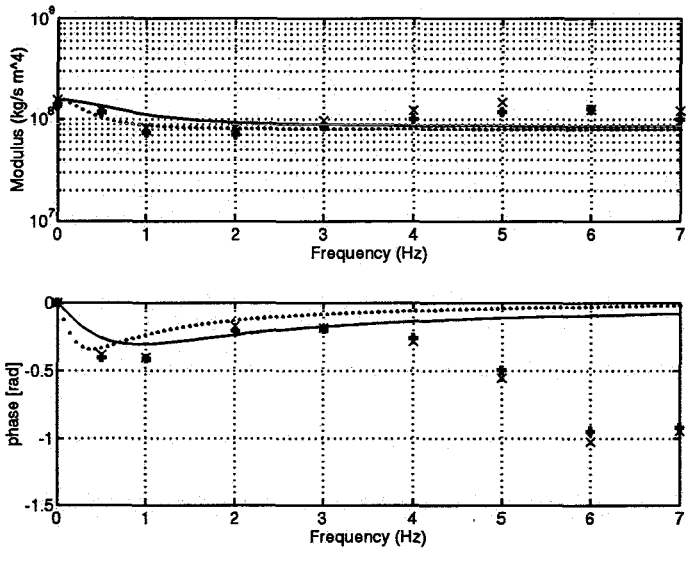

Figure B.9: *Impedance determined for flow amplitudes of 8 ml/s (+), 16 ml/s (x) and 24 ml/s (o); theoretical impedance (dotted line) and impedance fit (solid line). Modelparameters are listed in table B.2.*

Appendix C

Principles of laser-Doppler techniques

C.1 Laser-Doppler Anemometer

Laser-Doppler anemometry is based on the principle that two incoming coherent monochromatic light beams form interference fringe planes in the intersection region (measurement volume). When a (fluid) particle moves through the measurement section (with velocity $\vec{u} = (u_x, u_y, u_z)$), light is scattered from the particle, see figure C.1. This causes a frequency shift between the incident beam (wave vector $\vec{k_i}$) and scattered light beam (wave vector $\vec{k_s}$), the *Doppler shift*. The Doppler shift is given by the relation:

$$\omega_D = \vec{u} \cdot (\vec{k_s} - \vec{k_i}) \tag{C.1}$$

In practice, the splitting of the incident beams and the recombination of the scattered beams can be arranged in different ways or modes. In the experiments described in this report the *reference beam* mode is used. In this mode, the light scattered from the illuminating beam is combined with a reference beam, which is taken directly from the incident beam by means of a beamsplitter. To ensure a stable optical setup, the reference and laser beam illuminating the particles are focussed into the measurement volume by one common lense system. The light scattered from the particles in the direction of the reference beam and the reference beam

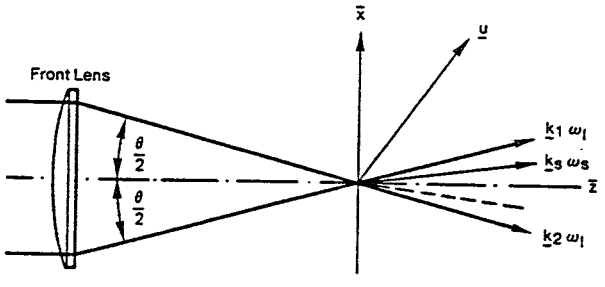

Figure C.1: *Vector diagram (from [Disa]).*

interfere on the diode detector surface, and the frequency difference is present in the detector current. In the coordinate system shown in figure C.1, the Doppler frequency is given by:

$$f_D = \frac{2u_x}{\lambda} \sin(\frac{\theta}{2}) \tag{C.2}$$

where θ is the angle between the incident beams. When the reference beam and laser beam have the same frequency, the Doppler-shift is independant of the direction of motion of the particles. Therefore a fixed frequency difference between reference beam and laser beam is introduced (40 MHz), the optical frequency shift. Furthermore a stable, selectable offset frequency can be introduced. The Doppler shift will add or subtract from this shift. As long as the shift is higher than the highest negative Doppler shift, the signal processor will be able to distinguish between negative and positive flow directions.

The performance of the LDA is described by some important parameters, which are shown in figure C.2. The measuring volume is ellipsoidal and its dimensions are given by:

$$d_x = \frac{d_f}{\cos(\frac{\theta}{2})} \tag{C.3}$$

$$d_y = d_f \tag{C.4}$$

$$d_z = \frac{d_f}{\sin(\frac{\theta}{2})} \tag{C.5}$$

where θ is the beam intersection angle and d_f the diameter of the focussed laser beam, see figure C.2. In the LDA experiments described in this report the parameters are:

laser wavelength	632.8 nm
beam expansion factor	1
focal length of front lens	80 mm
beam separation at front lens	39 mm
beam intersection angle	27.4 degrees
fringe separation	1.336 μm
number of fringes	60
waist at probe volume	80 μm
z-size of probe volume	330 μm
y-size of probe volume	80 μm
x-size of probe volume	80 μm

The seeding particles can be considered to be the actual velocity probes. The particles must be small enough to track the flow accurately, yet large enough to scatter sufficient light.

C.2 Vibrometer

The laser vibrometer is a special backscatter reference beam laser Doppler system. This system measures the on-axis velocity of vibrating solid surfaces. The illuminating beam is focussed on the solid surface. The backscattered light is collected by the same lens and combined with a reference beam coming directly from the laser, see figure C.3. The Doppler frequency is given by ($\theta \cong \pi$):

$$f_D = \frac{2V_z}{\lambda} \tag{C.6}$$

where V_z is the velocity of the object along the axis.

LDA

Doppler frequency: $f_D = \frac{2u_x}{\lambda}\sin\frac{\theta}{2}$ Calibration factor: $C = \frac{\lambda}{2\sin\frac{\theta}{2}}$

Diameter of focused laser beam: $d_f = \frac{4}{\pi}\frac{f\lambda}{Ed_i}$ Measuring volume dimensions: $d_x = \frac{d_f}{\cos\frac{\theta}{2}}$ $d_y = d_f$ $d_z = \frac{d_f}{\sin\frac{\theta}{2}}$

Fringe separation: $\delta_f = \frac{\lambda}{2\sin\frac{\theta}{2}}$ Fringe number: $N_f = \frac{8}{\pi}\frac{f}{Ed_i}\ tg\frac{\theta}{2} = \frac{4}{\pi}\frac{D}{d_i}$

Nomenclature:

λ	– laser wavelength
E	– beam expansion factor
d_i	– diameter of laser beam waist before expansion
d_f	– diameter of focused laser beam
D	– beam separation before expansion
θ	– beam intersection angle
f	– focal length of front optics
$\underline{u}$	– velocity vector $=(u_x, u_y, u_z)$
u_x	– velocity component in measuring direction

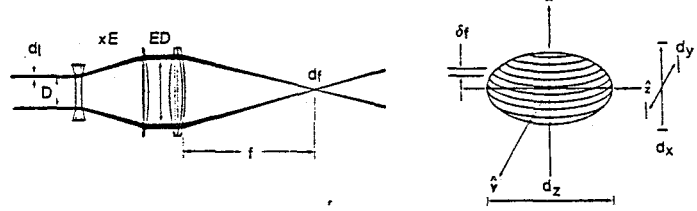

Figure C.2: *Optical parameters in laser-Doppler anemometry (from [Disa]).*

Laser vibrometer.

$$d_f = \frac{4}{\pi}\frac{f\lambda}{d_i}\frac{f_1}{f_2}$$

$$l_f \cong \frac{8}{\pi}\frac{f^2\lambda}{d_i s_1}\left(\frac{f_1}{f_2}\right)^2$$

$$f_D = \frac{2V_z}{\lambda}$$

Nomenclature:

f_D	– Doppler frequency
d_f	– diameter of focal spot
l_f	– length of focal region
f	– measuring distance
f_1, f_2	– focal lengths internally
d_i	– laser beam waist diameter
s_1	– internal beam separation
v_z	– velocity of object along axis
λ	– laser wavelength

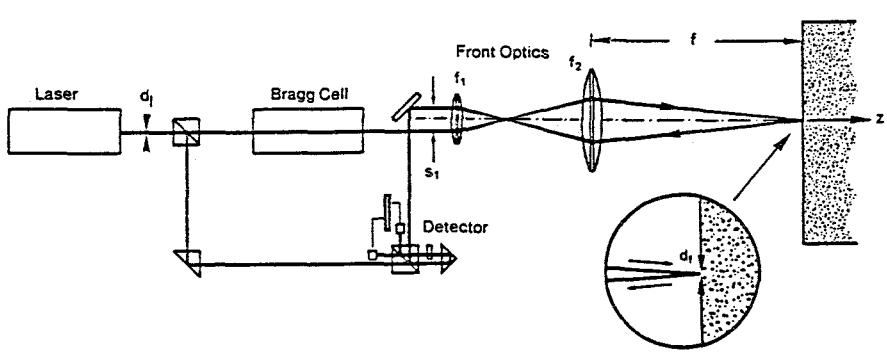

Figure C.3: *A schematic drawing of the laser-vibrometer (from [Disa]).*

Appendix D

Principles of ultrasound

Ultrasound is a high frequency wave (2–10 MHz) and is used in clinical practice for example to measure blood velocity. The ultrasound wave is generated with a piezoelectric crystal which convert an electrical signal to an ultrasound wave. This can be a continuous or pulsed wave. Ultrasound waves returned from inside the body (or from the experimental setup) consist of reflected and scattered ultrasound waves. Reflections occur at a boundary of which the dimension is greater than the wavelength of the ultrasound wave. The blood vessel wall for example is a good reflector. If the dimension of the boundary becomes small compared to the wavelength of the ultrasound wave, the wave will be scattered. Scattering will take place for example from blood particles.

In order to measure velocity distributions in blood vessels, a pulsed ultrasound wave is necessary. Pulsed wave systems transmit a burst (a number of periods) of ultrasound periodically. The time delay between these bursts determines the depth of measurement and the maximally detectable fluid velocity. The ultrasound transmitting crystal is then also used as receiver. The received ultrasound waves are transformed to radio frequent signals (RF-signals) in the piezoelectric crystal, see figure D.1. A single RF-signal consists of reflected waves, scattered waves, secondary reflected waves and noise. The power spectral density distribution of a RF-signal shows that: (1) reflections show a high spectral power, narrow bandwith, and low temporal mean frequency; (2) scattered waves show a low spectral power, wide bandwith, an temporal mean frequency depending on fluid velocity. The RF-signal is processed in the time domain to determine fluid velocity. A filter is used to discriminate between reflections and scattering, and a time domain mean frequency estimator is used for the estimation of the temporal frequency (Doppler frequency) and spatial mean frequency (carrier frequency).

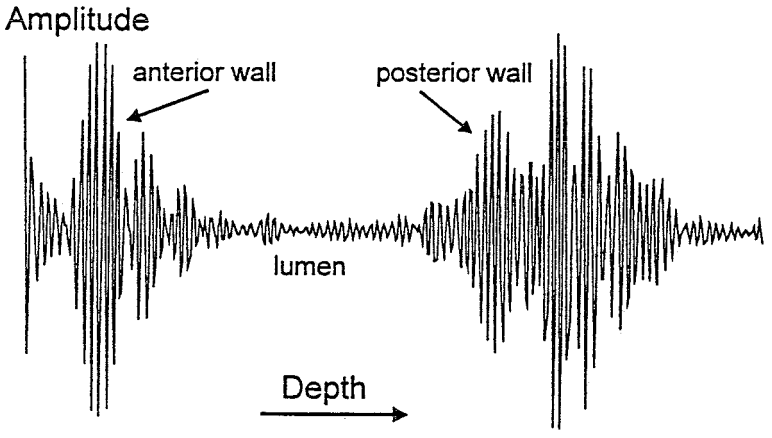

Figure D.1: *An example of a RF-signal received from the intersection of the ultrasound beam and a blood vessel.*

Appendix E

Impedance data

This appendix shows input impedance determined from measured pressure and velocity at several locations in the human arterial system. The data have been taken from [Mil70] and were converted into impedance in terms of pressure and flow using the internal radius of the artery in question. Data on internal radii have been taken from [Wes69].

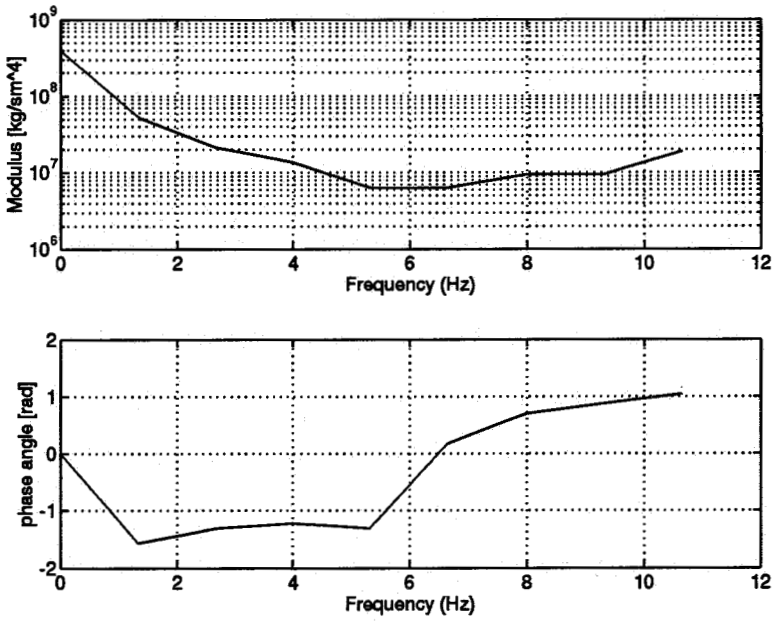

Figure E.1: *Modulus and phase of the input impedance for the descending aorta (T7). The internal radius of the artery was taken as 1.0 cm.*

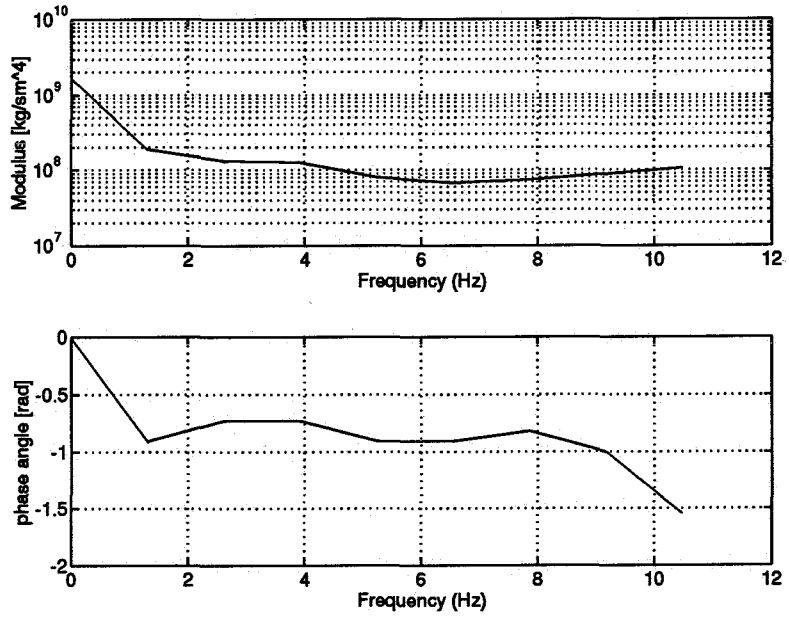

Figure E.2: *Modulus and phase of the input impedance for the abdominal aorta (L1). The internal radius of the artery was taken as 0.58 cm.*

Appendix F

List of symbols

Symbol	explanation	units
A	cross-sectional area	m^2
α	Womersley-parameter	-
c_o	Moens-Korteweg wave speed	ms^{-1}
C'	compliance per unit length	$m^3s^2kg^{-1}$
C	volume compliance	$m^4s^2kg^{-1}$
η	dynamic viscosity	kg m^{-1} s^{-1}
E	Young's modulus	Pa
f_{heart}	heart rate	Hz
F_{10}	Womersly function	-
Γ	reflection coefficient	-
h	wall thickness	m
k	wave number	m^{-1}
k	specific permeability	m^4
λ	wavelength	m
L	inertance	kg m^{-4}
L'	inertance per unit length	kg m^{-5}
ν	kinematic viscosity ($=\eta/\rho$)	m^2s^{-1}
ω	angular frequency	rad·s^{-1}
p	pressure	Pa
Q	flow	m^3s^{-1}
r	radial coördinate	m
R	vessel radius	m
R	resistance	$kgm^{-4}s^{-1}$
R'	Poiseuille resistance per unit length	$kgm^{-5}s^{-1}$
R_p	peripheral resistance	$kgm^{-4}s^{-1}$
ρ	density (of blood)	kgm^{-3} (1050 kgm^{-3})
τ	wall shear stress	kg m^{-1} s^{-2}
t	time	s
u_x	axial velocity	ms^{-1}
u_r	radial velocity	ms^{-1}

Symbol	explanation	units
Z_i	input impedance	$\mathrm{kgm^{-4}s^{-1}}$
Z_C	characteristic impedance	$\mathrm{kgm^{-4}s^{-1}}$
Z_{im}	input impedance of arterial segment	$\mathrm{kgm^{-4}s^{-1}}$
Z_{term}	terminal impedance	$\mathrm{kgm^{-4}s^{-1}}$
Z'_L	longitudinal impedance per unit length	$\mathrm{kgm^{-5}s^{-1}}$
Z'_T	transverse impedance per unit length	$\mathrm{kgm^{-3}s^{-1}}$